Syn-extensional emplacement of porphyry Cu-Mo and epithermal mineralization: the Zijinshan district, SE China

José Piquer[1, 2, *], David R. Cooke[1, 3], Jing Chen[1, 3], Lejun Zhang[1, 3]

[1]CODES, University of Tasmania, Private Bag 79, Hobart, Tasmania, 7001, Australia

[2]Instituto de Ciencias de la Tierra, Universidad Austral de Chile, Edificio Pugín, Av. Eduardo Morales Miranda, Valdivia, Chile

[3]TMVC (Transforming the Mining Value Chain), an Australian Research Council Industrial Transformation Research Hub, University of Tasmania, Private Bag 79, Hobart, Tasmania, 7001, Australia

**Corresponding author: e-mail, jose.piquer@uach.cl*

Abstract

The Zijinshan district, Fujian Province, SE China, is a major mineral field that contains high- and intermediate-sulfidation epithermal Cu-Au-Ag and porphyry Cu-Mo deposits. This contribution discusses the structural geology and the tectonic regime prevalent during mineralization at Zijinshan. Statistically, the district is dominated by NW-striking fault systems which dip at moderate angles (40-50°) to the NE and SW. They played a first-order role in controlling the emplacement of hydrothermal veins and breccias. Most NW-striking faults were active as oblique normal/strike-slip faults during mineralization, as evidenced by the geometry of syn-tectonic hydrothermal mineral fibres. NE-striking, steeply-dipping faults also controlled the emplacement of hydrothermal veins and breccias, and contain syn-tectonic mineral fibres indicating predominantly dextral strike-slip movements. The kinematic and dynamic analysis of fault-slip data shows that the predominant tectonic regime during mineralization was extensional, with subvertical σ_1 and NNE- to NNW-trending σ_3. Secondary clusters of subhorizontal σ_1 suggest that short periods of fault reactivation under a strike-slip regime occurred locally. Although the formation of porphyry Cu-Mo systems is commonly thought to be favoured by compressive to transpressive tectonic regimes, which lead to a diminution in the rate of volcanic output and to the entrapment of magmas and volatiles in the upper crust, these results show that at least medium-sized porphyry Cu-Mo systems can form under extensional conditions in previously-thickened continental crust. This has important exploration implications globally. Based on the current geological knowledge, the district appears to have a high exploration potential at depth, mainly for IS epithermal and porphyry-style mineralization.

Introduction

Porphyry deposits are the world's primary source of Cu and Mo, including the largest known economically exploitable accumulations of both elements (Rio Blanco-Los Bronces and El Teniente, central Chile; Sillitoe, 2010). It has long been recognized that most of the giant porphyry deposits, in particular porphyry Cu-Mo deposits, were formed in convergent magmatic arcs under compressional to transpressional conditions, commonly after continental-scale events of crustal thickening, shortening, uplift and exhumation (e.g. Cooke et al., 2005; Sillitoe, 2010).

This work discusses the district-scale structural geology and explores the tectonic regime prevalent during formation of the Zijinshan mineral district. Zijinshan is a major camp of high- to intermediate-sulfidation epithermal Cu-Au-Ag and porphyry Cu-Mo deposits located in the mountains of Fujian Province, SE China, approximately 15 km to the north of the town of Shanghang (Fig. 1). It is the largest epithermal mining district in China (Mao et al., 2007). The district include the Zijinshan open pit Cu-Au mine, which exploits a high-sulfidation epithermal system and the Yueyang underground Ag-Cu-Au mine, which exploits intermediate-sulfidation veins about 5 km to the SW of the Zijinshan open pit (Fig. 1). The Zijinshan Cu-Au deposit is the largest in China, with a total resource of 1.9 Mt Cu and 305 t Au and an annual production of 16 t Au (Jiang et al., 2013). The district also contains porphyry Cu-Mo prospects at Luoboling and Wuziqilong; porphyry to high-sulfidation epithermal prospects at Longjiangting and Ermiaogou; a high-sulfidation prospect at Dajigang, and an intermediate-sulfidation prospect at Gushibei (Fig. 1). The entire Zijinshan district is estimated to contain 2.36 Mt Cu, 323 t Au, 1,554 t Ag and 4,647 t Mo (Zhong et al., 2014).

Several models have been proposed for the tectonic context of the deposits in the district, including the studies of Feng (1993), So et al. (1998) and Jiang et al. (2015), who concluded that Cretaceous magmatism coeval with hydrothermal activity at Zijinshan occurred in a subduction setting under extensional conditions, associated with a steepening subduction angle. Chavret et al. (1994), instead, proposed the existence of a short-lived compressive event coeval with mineralization. Existing geological maps (e.g., So et al., 1998; Jiang et al., 2013) show two almost orthogonal sets of structures at Zijinshan, with broadly NW and NE strikes, and previous studies have highlighted the preferred NW trend evident in several veins and breccia dikes at Zijinshan (e.g., So et al., 1998). However, no specific studies have been completed regarding the district's structural evolution. Problems such as fault kinematics, stress state during faulting and mineralization and the detailed relationships between specific structures and hydrothermal fluid flow have not been addressed previously. This study discusses these topics based on kinematic and dynamic analysis of new fault-slip data and the study of syn-tectonic hydrothermal veins.

Geological framework

The tectonic, magmatic and metallogenic history of south-eastern China has been the subject of several previous studies. A summary of these results is presented here, with an emphasis on the Mesozoic magmatic and tectonic events with which the mineralization of the Zijinshan district is related. Table 1 summarizes the ages of the main magmatic and hydrothermal events recognized in the area covered by this study.

The rocks of south-eastern China constitute the South China block, which is composed of the Yangtze craton and the Cathaysia block. The latter is a smaller continental terrane which contains the Zijinshan district (Fig. 2). The Cathaysia block was first accreted to the south-eastern margin of the Yangtze craton during the Proterozoic (Zhou et al., 2002; Pirajno and Bagas, 2002). The boundary between the Yangtze craton and the Cathaysia block is defined by the Jiangshan – Shaoxing and Pingxiang – Yushan sutures (Li and Jiang, 2014), which contain bands of ophiolite and high-pressure metamorphic rocks (Pirajno and Bagas, 2002 and references therein).

During the Triassic, the rocks of the South China Block were affected by a major period of tectonism and magmatism, the Indosinian Period. Deformation was associated with the collision of the South China Block and the Indochina Block to the south, and the North China Craton to the north (Fig. 2; Zhou et al., 2006; Mao et al., 2013). These collisional events are part of the large-scale Tethyan tectonism, characterized by the northward-movement of continental blocks leading to the amalgamation of Eurasia, forming broadly E-W trending orogenic systems and magmatic belts.

The earlier Indosinian granitoids have gneissic and mylonitized textures, and are interpreted as syn-collisional granites emplaced during amalgamation between the Indochina and South China blocks (Zhou et al., 2006). However, about 90% of the Indosinian granitoids were emplaced in the Late Triassic and show no evidence of deformation occurring during emplacement. Consequently, they are interpreted as post-collisional granites, which were emplaced in localized extensional sites (Zhou et al., 2006).

Since the Jurassic, the Cathaysia block has been dominated by Pacific tectonism, i.e., by the oblique subduction of the paleo-Pacific Plate beneath the south-eastern margin of Eurasia (Pirajno and Bagas, 2002; Zhou et al., 2006; Mao et al., 2007, 2013). The change from Tethyan to Pacific tectonism in SE China marks the initiation of the Yanshanian tectono-magmatic period, characterized by the formation of a wide NE to NNE-trending magmatic belt in the continental margin, which includes the Coastal Volcanic Belt (Fig. 2), and an associated deformation zone affecting the entire Cathaysia block known as the South China Fold Belt (Pirajno and Bagas, 2002).

The Yanshanian period can be subdivided into two main stages: Early Yanshanian (180-142 Ma) and Late Yanshanian (142-67 Ma; Zhou et al., 2006). The Mid- to Late Jurassic granitoids and volcanic rocks of the Early Yanshanian are distributed over a wide area, up to 800 km away from the present-day coastline. The plutonic rocks correspond mainly to calc-alkaline granites. Volcanic rocks of this stage have a narrower age range (180-170 Ma) than the granites and show a bimodal composition (Zhou et al., 2006). Most of the rocks cropping out in the Zijinshan district correspond to granites emplaced during the Early Yanshanian. These rocks host a significant proportion of the mineralized veins and breccias in the Zijinshan epithermal Cu-Au deposit (So et al., 1998; Mao et al., 2007). According to existing U-Pb zircon ages, all of the Early Yanshanian granites of the Zijinshan district were emplaced during a short time period, between 165 and 157 Ma (Jingmei, Wulongzi and Jinlongqiao granites; Jiang et al., 2013). The tectonic regime prevalent during the Early Yanshanian is still a matter of debate. Most authors propose a predominantly compressive regime, associated with the formation of the South China Fold Belt during this time (e.g., Wu et al., 1998; Zhang et al., 2001).

The Late Yanshanian rocks can be subdivided into an Early Cretaceous suite of volcanic and intrusive rocks associated with continental margin calc-alkaline magmatism, and a Late Cretaceous package comprising tholeiitic basalts intercalated with red beds that were deposited in continental back-arc basins formed as active subduction retreated towards the east (Zhou et al., 2006). The early Late Yanshanian magmatism was localized in a narrower belt than the Early Yanshanian, and magmatic activity occurred closer to the continental margin. Some authors have associated this with a progressively steeper subduction angle of the Pacific Plate below Eurasia during the Cretaceous (e.g., Zhou and Li, 2000). The Late Yanshanian appears to represent a transition from compressional to extensional conditions, with an extensional regime well established in the Late Cretaceous (Zhou et al., 2006) associated with a retreating trench, steepening subduction angle and the opening of back-arc basins. Some authors have proposed the existence of a short-lived contractional period at ~100 Ma, associated with N- to NNW-directed compression, reflected as an unconformity between Cretaceous volcanic sequences (e.g., Charvet et al., 1994). This postulated contractional period is broadly coeval with mineralization in the Zijinshan district (porphyry-style mineralization dated at 106-103 Ma, Re-Os ages in molybdenite, and intermediate-sulfidation epithermal mineralization dated at 97-91 Ma, $^{40}Ar/^{39}Ar$ ages in adularia; Zhang et al., 2003; Liu and Hua, 2005; Zhong et al., 2014).

Porphyry-style and epithermal mineralization in the Zijinshan district is genetically associated with Late Yanshanian magmatism. Intrusive rocks emplaced during this period included the Sifang granodiorite (112 ± 1 Ma; U-Pb in zircon, Jiang et al., 2013), dacitic domes and dikes (110-104 Ma; U-Pb in zircon ages, Jiang et al., 2013), the Luoboling granodiorite porphyry (106-103 Ma; whole rock Rb-Sr and U-Pb in zircon ages, Zhang et al., 2001; Li and Jiang, 2015), mineralised hydrothermal breccias and the mainly post-mineral syenite and quartz-monzonite dikes (100-92 Ma; U-Pb in zircon ages, Li and Jiang, 2014).

Thick sequences of Late Yanshanian volcanic and sedimentary rocks, which constitute the Shimaoshan Group (Feng, 1993), were accumulated within the Shanghang volcano-tectonic basin in the south-western part of the district (Jiang et al., 2015). The Shanghang basin forms part of a series of Cretaceous volcano-sedimentary basins developed across the region (Fig.

2B). The lower part of the basin infill is predominantly volcanic, while the younger part of the sequence is composed mostly of clastic units (Jiang et al., 2015). Available U-Pb zircon ages of volcanic rocks range between 110 and 99 Ma (Jiang et al., 2013, 2015). They are coeval with the emplacement of porphyritic intrusions and porphyry-style mineralization.

Regional- and continental-scale structures that were active during the Yanshanian in the Cathaysia block have predominantly NE and NW strikes (Fig. 2). NE-striking structures are parallel to the Yanshanian magmatic arc and to the continental margin. The NW-striking faults are highly oblique to the Pacific margin but they are parallel to the structures associated with the Tethyan-Himalayan deformation events. The local structural geology of the Zijinshan district is dominated by similar sets of NE- and NW-striking faults (So et al., 1998; Jiang et al., 2013; Lai and Qi, 2014; Chen et al., 2015). The Jurassic plutonic rocks of the district are interpreted to have been emplaced at the core of a regional scale, NE-striking anticline (the Xuanhe Anticlinorium, Fig. 2B), parallel to sets of faults with similar orientations (Lai and Qi, 2014). The NW-striking faults, in turn, controlled the emplacement of most of the hydrothermal breccias and veins that host high-grade Cu-Au mineralization in the Zijinshan epithermal deposit (So et al., 1998).

Methodology

Structural, lithological and mineralogical information was collected across the Zijinshan district during one month of field work completed in November, 2014. Structural stations were distributed across the study area (Fig. 3). At each structural station, the strike and dip of every observed fault plane were measured. When present, the pitch of fault plane striations and slickenfibres were also measured. Kinematic criteria for brittle faults (e.g., Petit, 1987) was used to establish the sense of movement, and the type of kinematic indicator used was always recorded. Steps in slickenfibres were the most common indicator, followed by other criteria such as syn-tectonic minerals precipitated in strain fringes, dilational jogs filled by hydrothermal minerals, displacement of markers and P-only surfaces (Petit, 1987). A total of 548 fault planes were measured, and 152 of them (~30%) yielded reliable kinematic information.

Predominant fault plane orientations were studied using the Stereonet™ software (Allmendinger et al., 2012). Kinematic and dynamic analyses were completed for the 152 fault planes containing kinematic information. The fault-slip data was also analysed for specific areas within the district (Fig. 3), characterized by different lithological units and mineralization styles, in order to resolve spatial and temporal variations in the stress regime. Because most of the kinematic indicators used are given by syn-tectonic hydrothermal minerals, studying the conditions under which the faults were active allows the determination of the tectonic regime under which specific alteration and mineralization events occurred.

For the kinematic analysis of the fault-slip data, the FaultKin™ software (Marrett and Allmendinger, 1990; Allmendinger et al., 2012) was used to calculate the orientation of the pressure and tension axes for individual fault planes and the average kinematic axes (shortening, stretching and intermediate axes) for different groups of faults. For the dynamic analysis, the Multiple Inverse Method (Yamaji, 2000) was used to calculate the orientation of paleo-stress tensors from the inversion of fault-slip data. The advantage of this method is that it has the capacity to resolve different stress states from heterogeneous data sets. The program calculates the four parameters which define a stress state: the orientation of the three principal stresses and the stress ratio $\Phi = (\sigma_2-\sigma_3)/(\sigma_1-\sigma_3)$. The stress ratio varies from 0 to 1, and describes the geometry of the stress ellipsoid. If the magnitude of σ_2 is similar to the magnitude of σ_1, the stress ratio would approach 1; similarly, a stress ratio approaching 0 means the magnitudes of σ_2 and σ_3 are similar. These parameters are calculated for all the possible groups of a given number of faults, taken from the fault-slip database. The number of faults contained in each group is referred to as the fault combination number k, and can be chosen by the user. The software developers recommend $k = 5$, or $k = 4$ for large datasets (more than 122 fault planes). A larger k value does not significantly change the results, while for $k < 4$ the inversion solution is an under-determined problem. The optimal stress tensor for each of the groups of k fault planes is calculated using classical stress inversion methods based on the Wallace-Bott hypothesis (Wallace, 1951; Bott, 1959). The software does so attempting to minimise the misfit angle, which is defined as the angle between the observed and theoretical slip direction on a fault plane under a given stress state. If for a given group of k faults the misfit angle in at least one fault is greater than 20° for every possible stress state, that group is discarded and said to be incompatible. An optimal stress tensor, then, is defined as one for which the misfit angle is smaller than 20° for each of the k faults contained in the respective group. All the calculated optimal stress tensors can be visualized as paired stereoplots for σ_1 and σ_3. If all of the calculated optimal stress orientations for the different groups of k faults plot in a single cluster, then the fault-slip data are homogeneous and fault movement can be explained by a unique state of stress. If different clusters of stress orientations are observed in the stereoplots, then the data are heterogeneous, and each cluster would represent a different stress state.

An updated geological map of the Zijinshan district has been prepared, based on new data collected during this study, the existing geological map of the district compiled by the Zijin Mining Group Co and the analysis of satellite images. A simplified version of this map is presented in Figure 4. The updated geological map was used to prepare a SW-NE long section across the Zijinshan district (Fig. 5). The section passes through the areas of Bitian, Dajigang, Zijinshan and Luoboling (Fig. 4). The geological map and cross-section were prepared in the software ArcMap.

Syn-tectonic hydrothermal and magmatic activity

Across the Zijinshan district, there is abundant evidence of a strong relationship between faulting and hydrothermal activity. Fault planes are decorated by a wide range of syn-tectonic hydrothermal minerals, including alunite, dickite, quartz, muscovite, illite, kaolinite, calcite, chlorite and hematite (Fig. 6). These syn-tectonic hydrothermal minerals can be found in all of the major mineralised centres of the district, and belong to a wide variety of alteration stages.

Faults have also controlled the geometry of alteration and mineralization zones (Fig. 7) and the formation of abundant tectonic-hydrothermal breccias, which are very common throughout the district, particularly at Zijinshan and Dajigang (Fig. 8). In those two areas, tectonic-hydrothermal breccias strike predominantly to the NW, but they dip to the NE at Zijinshan and to the SW at Dajigang (Figs. 5, 8A). The breccias contain clasts of different intrusive rocks commonly altered to dickite and alunite and also clasts of older hydrothermal veins, cemented by hydrothermal minerals such as covellite, digenite, pyrite and alunite. The tectonic character of the hydrothermal breccias is evident when they displace older generations of veins and breccias (e.g., Fig 8B) and also by the presence of syn-tectonic mineral fibres at their contacts. The relatively low angle of the breccia bodies and their strong structural control suggest that the brecciation process was mainly tectonic instead of hydraulic fracturing, although fault slip and tectonic brecciation were probably assisted by syn-tectonic hydrothermal fluid flow.

There is local evidence of magmatic foliation in the margins of dikes emplaced along faults (Fig. 9). This indicates syn-tectonic emplacement of at least some magmatic bodies.

Syn-tectonic volcano-sedimentary units

The volcaniclastic deposits and lava flows of the Cretaceous Shimaoshan Group were accumulated in a series of fault-bounded depocentres that crop-out mainly to the SW of the NW-striking, SW-dipping F 2-1 fault (Fig. 4). The volcanogenic sedimentary intercalations found in the hanging wall of the F 2-1 fault system form growth-strata, and thicken toward the NE (Fig. 10A). This geometry suggests syn-tectonic deposition of the volcaniclastic sediments during normal movement of the F 2-1 fault system and parallel faults (Fig. 10B).

To the south-west, the opposite basin boundary is defined by the Shanghang-Yunxiao Fault (Fig. 2B), located outside the area covered by this study. The presence of growth strata thickening toward the SW (Fig. 10C) suggest the presence of NE-dipping growth faults, possibly parallel to the Shanghang-Yunxiao Fault.

Analysis of fault plane data

The rose diagram of Figure 11A illustrates the dip directions of the 548 faults contained in our structural database. Consistent with the district-scale fault architecture illustrated by Figure 4, a strong preferred NW strike is evident, with two populations dipping to the NE and to the SW respectively. Secondary populations include NE- and E-striking faults. The NE striking faults dip preferentially to the NW, while most E-striking faults dip to the south.

Figure 11 also shows the results of the kinematic (Fig. 11B) and dynamic (Fig. 11C) analysis for the entire Zijinshan district, using the 152 faults for which it was possible to establish the sense of movement by the use of kinematic indicators. The results show that the kinematics of most fault planes is consistent with fault activity under an extensional regime: both the average shortening axis and the main cluster of σ_1 are subvertical, while the average stretching axis and the main cluster of σ_3 are subhorizontal and indicate a predominant NNE direction of extension, parallel to the continental margin.

However, the dynamic analysis using the Multiple Inverse Method show some secondary clusters that diverge from the main trends. Two groups of faults are consistent with low angle σ_1 and σ_3, trending WNW and NNE respectively, indicating that a small number of faults were active under a stike-slip regime (Fig. 11C). The plot for σ_3, in turn, shows that while most of the faults are consistent with NNE-directed extension, there is a high variability in the extension direction, with several groups of faults consistent with N- and NNW-trending σ_3 (Fig. 11C). These might be explained by the fact that most if these groups of faults have stress ratios close to 0 (violet and blue colors in Fig. 11C), indicating that σ_2 and σ_3 have similar magnitudes, preventing the software from distinguishing appropriately between the intermediate and minimum principal stresses.

Yueyang, Bitian and Gushibei

The surface outcrops of these three areas correspond to volcanic rocks of the Cretaceous Shimaoshan Group (Fig. 4). They contain epithermal veins, mainly of intermediate sulfidation state, associated with Ag-Au-Cu mineralization. Some of the veins are currently being exploited by the Yueyang underground mine (Fig. 1). The thickness of the Cretaceous volcano-sedimentary rocks is highly variable, as shown by drill holes and by the exposures in the tunnels of the Yueyang underground mine. The volcanic rocks are underlain by Jurassic intrusive rocks in the area of Yueyuang, which have a sill-like geometry with variable thickness. Below the Jurassic intrusions are Neoproterozoic phylites. The contacts between different lithological units were observed during this study, both in drill core and in the mine tunnels. In all the studied cores and localities the contacts correspond to low-angle faults, commonly controlling the emplacement of veins and tectonic-hydrothermal breccias. Some of them may correspond to primary intrusive or stratigraphic contacts that were later reactivated as faults.

Faults in the three areas have a strongly preferred NW strike, but there are variations in the dip direction (Figs. 12A, 13A). At Yueyang, most of the NW-striking faults dip to the NE. At Bitian, most faults also dip to the NE, but there is a major group of faults dipping to the SW. In Gushibei, NW-striking faults dip preferentially to the SW (Figs. 6B, 12A), parallel to the fault contact between the Cretaceous sequences and their basement (F 2-1 fault, Fig. 4).

Only two faults with reliable kinematic indicators were found in Gushibei, and four in Yueyang. These numbers are not enough for the calculation of paleo-stress tensors with the Multiple Inverse Method. Because of this, they were grouped with the faults measured in the Bitian area, where it was possible to obtain the sense of movement for 10 faults. The results of the kinematic and dynamic analysis for the three areas (16 faults in total) are shown in Figure 12B, C. The average kinematic axes suggest extensional conditions, with subvertical shortening and a stretching direction trending NNE (Fig. 12B). However, there is a large variability in the orientation of the pressure axes (blue dots). This suggests that different groups of faults were active under different stress regimes. This situation is properly solved by the Multiple Inverse Method (Fig. 12C), where two different stress tensors emerge: one is extensional, with vertical σ_1 and E-W σ_3, and the other one indicates a strike-slip regime, with WNW-trending σ_1 and NNE-trending σ_3. Both clusters are supported by several groups of faults.

Longjiangting and Ermiaogou

This area is located in the north-western corner of the Zijinshan intrusive complex (Fig. 4), and contains outcrops of the Jurassic Jingmei, Wulongzi and Jinlongqiao granites. To the NNE, intrusive rocks are in fault contact with the Neoproterozoic basement, whereas to the SW the intrusions are in fault contact with the Cretaceous Shimaoshan Group. The Jurassic plutons are cut by a series of tectonic-hydrothermal breccias, which preferentially strike NW and dip to the NE. The preferred dip direction of fault planes in this area is also to the NE (Fig. 14A). A secondary population of faults strike NE, parallel to the contact between the Jurassic intrusions and the Neoproterozoic basement, and dip both to the NW and SE.

Both the kinematic and the dynamic analysis indicate fault activity occurred under an extensional regime, with vertical shortening axis and σ_1 (Fig. 14A). The average stretching axis and the main cluster of σ_3 indicate an ENE-trending extension direction, but both the calculated tension axes for individual fault planes and σ_3 for individual groups of faults show a large variability (Fig. 14A).

Dajigang and Sanqingting

Outcrops in this area are dominated by the Jurassic Jingmei and Wulongzi granites, which have been intruded by Cretaceous dacitic dikes and NW-striking, SW-dipping tectonic-hydrothermal breccias (Figs. 5, 8A, 13B) with local Au mineralization. The area lies adjacent to the NE of the faulted contact between the Jurassic plutons and the Cretaceous volcano-sedimentary rocks of the Shimaoshan Group.

The rose diagram for the dip direction of faults (Fig. 14B) shows a major population of faults striking NW and dipping to the SW, parallel to the hydrothermal breccias of the area and to the main fault (F 2-1) which juxtaposes the Jurassic intrusive complex with the Shimaoshan Group. The damage zones of individual NW-striking faults are up to 4 meters wide. A second group of faults strikes E and dip to the south (Fig. 14B). Fault plane kinematics are consistent with an extensional regime, with a subvertical orientation of the main cluster of σ_1 and the shortening axis (Fig. 14B). As in other areas, extension direction is subhorizontal but the trend is highly variable; the main cluster of σ_3 trends to the WNW (Fig. 14B).

The results of the Multiple Inverse Method show a very minor cluster of faults which were active under a strike-slip regime, with σ_1 subhorizontal and trending almost N-S (slightly NNE) and σ_3 also subhorizontal and trending E-W to WNW (Fig. 14B).

Zijinshan

This area is located in the central part of the Zijinshan intrusive complex (Fig. 4). The main lithologic unit is the Jurassic Wulongzi granite, which has been intruded by Cretaceous dacitic domes and dikes (Fig. 4) and by hydrothermal and tectonic-hydrothermal breccias. Most of the Cu and Au mineralization of the Zijinshan deposit is contained in tectonic-hydrothermal breccias and parallel veins, which strike preferentially to the NW and dip moderately to the NE (So et al., 1998; this study). The mineralised breccias and veins contain a typical high-sulfidation mineral assemblage, dominated by Cu sulfides such as covellite, digenite and enargite, associated with dickite and alunite alteration (Chen et al., 2015; this work).

The study of fault plane orientation shows that faults at Zijinshan preferentially strike NW and dip to the NE (Fig. 14C), including the main faults observable in the open pit mine (Fig. 15). An important secondary population of faults strike NE and dip to the NW (Fig. 14C).

The kinematic and dynamic analysis shows a consistent NNE direction of extension (stretching axis and σ_3) for syn-mineral faults within this area. The calculated orientations of σ_1 for different groups of faults, however, show larger variability (Fig. 14C). The main cluster plunges at a high angle and is consistent with extensional conditions during faulting. There are, however, secondary groups of faults with calculated σ_1 plunging at lower angles (Fig. 14C), which suggest fault activity under a strike-slip regime, with WNW-trending σ_1 and NNE-trending σ_3.

Luoboling and Wuziqilong

These two areas correspond to porphyry Cu-Mo prospects, partly exposed on the surface. They show typical porphyry-style alteration and mineralization at deeper levels, with a transition to epithermal-style advanced argillic alteration at higher elevations (Zhong et al., 2014). The surface outcrops correspond mostly to Cretaceous intrusive rocks (Fig. 4), the

Sifang granodiorite and the Luoboling granodiorite porphyry. There are also outcrops of the Jurassic Wulongzi granite in the north-western part of the area. All of these units are cut by dacitic and syenitic dikes and by tectonic-hydrothermal breccias.

Faults in the area predominantly have a NW strike (Fig. 16), with similar populations dipping to the NE and SW (Fig. 14D). A secondary population of E-striking faults dip preferentially to the N. NE-striking faults are minor and dip both to the NW and SE (Fig. 14D).

The kinematic and dynamic analysis reveals a predominantly extensional regime, with subvertical σ_1 and shortening axis and an extension direction trending NNW. The Multiple Inverse Method shows a very minor secondary cluster of orientations of σ_1, with a subhorizontal plunge and NNE trend. They are associated with subhorizontal, WNW-trending σ_3. This suggests that a small group of faults was active under a strike-slip regime.

NW and SE of Zijinshan

These two areas correspond to exploration prospects located close to the contacts between the Jurassic intrusive complex and the Neoproterozoic basement, to the NW and SE of the Zijinshan HS epithermal deposit (Fig. 4). At each prospect, only two fault planes yielded reliable kinematic indicators. This makes it impossible to complete a dynamic analysis using the Multiple Inverse Method.

In the NW area, the contact between the Jurassic intrusive rocks and the basement correspond to a major fault, which has controlled the formation of tectonic-hydrothermal breccias (F 1-1, Fig. 4). The fault strikes to the ENE, dips at high angles to the SSE and shows evidences of oblique normal-dextral movement. Consistent with that, the rose diagram for the dip direction of faults shows a predominant group of ENE-striking faults dipping to the SSE (Fig. 17), which correspond mainly to measurements of the main F 1-1 fault and parallel, subsidiary fault planes. A second group of faults strikes WNW and dips to the NNE (Fig. 17). The calculation of P and T axes for the two fault planes where it was possible to establish the sense of movement yielded different results (Fig. 17). For one of them the P axis plunges at low angle to the NNW, while the T axis plunges at high angle. For the other fault, both the P and T axes plunge at low angles, the P axis with a WNW trend and the T axis trending NNE.

The SE project is located at the southern boundary of the Jurassic intrusive complex (Fig. 4). The contact is poorly exposed, and its nature (intrusive or tectonic) is not clear. However, the presence of nearby faults striking parallel to the contact (Fig. 4) suggests that its nature might be tectonic, or an intrusive contact reactivated as a fault. Some of the published geological maps of the district show the SE project to be located on the trace of the NW-striking faults that controlled the emplacement of the breccias and veins at Zijinshan. This is erroneous, however, as because of the rugged topography, the trace of the faults on the surface is not parallel to their strike. The SE project is located at elevations ~700 m lower than Zijinshan, which means that the trace of the NW-striking faults of Zijinshan, which dip at moderate angles (40-50°) to the NE, pass several hundred meters to the NE of the area covered by the SE project (Fig. 4). Most fault planes in the SE project strike NW, but their dip direction is opposite to that of the faults at Zijinshan: they dip preferentially to the SW (Fig. 17). It is therefore concluded that the NW-striking faults at the SE project do not link up directly with those at Zijinshan (Fig. 4).

A secondary population of faults in the SE project strike ENE, parallel to the contact between intrusive and metasedimentary rocks. Similar numbers of ENE-striking faults dip to the N and to the S (Fig. 17). The two faults with reliable kinematic indicators have entirely different P and T axes: in one the P axis is subvertical and the T axis plunges at low angle to the NNW, while in the other one both the P and T axes plunge at low angles, with the P axis trending NNE and the T axis trending WNW (Fig. 17).

Discussion

As illustrated by Figures 4 and 11A, fault architecture in the Zijinshan district is dominated by NW-striking, moderately dipping faults. Apart from being statistically the predominant fault trend in the district, the NW-striking faults also form the best developed fault systems, such as the ones observed at Longjiangting, Dajigang and Zijinshan (Fig. 4), which are several hundred meters wide. NW-striking faults also controlled the geometry of the volcanic basin where the rocks of the Shimaoshan Group accumulated (Figs. 4, 10). Volcanic rocks deposited in this basin are coeval with mineralization in the district (Jiang et al., 2013; Zhong et al., 2014).

The different NW-striking faults in the district appear to correspond to conjugate faults active under transtension: they show predominantly normal movement coupled with a variable strike-slip component. In general, sinistral slip is predominant in NE-dipping faults, such as in the Zijinshan area, and dextral slip in the SW-dipping faults, such as in the Dajigang area; but there are several exceptions to this general trend. Some of the NW-striking fault systems show abrupt changes in dip direction. This probably reflects the presence of NE-striking faults acting as transfer faults and linking different segments of the basin-bounding, NW-striking faults. An example of this situation is found in the areas of Longjiangting and Dajigang-Sanqingting. These areas appear to be located on the same NW-striking fault system (Fig. 4). However, the faults dip to the NE in Longjiangting (Figs. 4, 14A) and to the SW in Dajigang-Sanqingting (Figs. 4, 14B). The change in dip direction occurs in the northern end of the Dajigang-Sanqingting area (Fig. 4), where the NW-striking faults intersect a NE-striking fault (equivalent to the F 1-4 fault, Fig. 4) and also an E-striking fault system.

A secondary group of faults striking NE is also evident in the Zijinshan district (Figs. 4, 11A). They generally dip at much higher angles than the NW-striking faults. They are more discontinuous and their damage zones and surface expression are more restricted than for the NW-striking faults (Fig. 4). Some of the NE-striking faults, such as the F 1-1 fault in the northern contact between the Jurassic intrusive complex and the basement (Fig. 4), controlled the emplacement of hydrothermal veins and mineralised tectonic-hydrothermal breccias. Localization of mineralization by these faults was, however, much less common than along the NW-striking fault systems. The geometry of syn-tectonic hydrothermal mineral fibres indicates that the sense of movement of NE-striking faults during mineralization was mostly dextral strike-slip.

The continental-scale structural architecture of SE China (Fig. 2A) is also dominated by NW- and NE-striking faults. They correspond to long-lived fault systems inherited from ancient orogenic events. The NW-striking faults of the Zijinshan district are located along-strike of continental-scale fault systems active during the Indosinian and older Tethyan orogenic events (Fig. 2). In particular, the trace of the NW-striking, continental-scale Shanghang-Yunxiao fault is located ~20 km to the west of the Zijinshan district (Fig. 2B). This fault system, similar to many of the smaller NW-striking faults of the Zijinshan district, was active as a basin-bounding fault during the Cretaceous (Fig. 2B). It is likely that the NW striking faults in the Zijinshan district inherited their orientations from ancient, repeatedly-reactivated, continental-scale weakness zones. The NE-striking faults, in turn, are parallel to the Jurassic-Cretaceous magmatic arc and to the main fold trends of the area. The Jurassic intrusive rocks of the Zijinshan district, in particular, were emplaced in the core of a NE-trending, regional-scale anticline, called the Xuanhe Anticlinorium by previous workers (e.g., Jiang et al., 2013; Fig. 2B). Some of the NE-striking faults of the district might have originated in the Jurassic as accommodation faults in the hinge of this anticline. This suggests that the local structural architecture of the Zijinshan district reflects the larger-scale structural grain, and the main faults active during mineralization correspond to local manifestations of continental-scale structures.

At the district scale, the tectonic regime prevalent during mineralization was extensional. This is in agreement with previous workers who documented extensional conditions during the Cretaceous along the SE China margin, associated with an increase in the angle of subduction of the Pacific Plate below Eurasia and a retreat of the trench towards the east (Zhou and Li, 2000; Zhou et al., 2006). The extension direction calculated from fault-slip data changes between NNW and NNE (probably reflecting local variations in the stress regime and/or uncertainties in the distinction between σ_2 and σ_3) but on average trends NNE (Fig. 11B, C). This implies that the NW-striking faults were more favourably oriented for dilation, explaining why their movement show a larger normal component and why they exerted a much stronger control on the formation of hydrothermal breccias and veins than the more purely strike-slip, NE-striking faults.

Despite the strong prevalence of extensional conditions during mineralization and fault activity in most of the Zijinshan district, there were clearly short-lived periods in which a strike-slip regime was predominant. This caused the reactivation of normal faults in strike-slip mode, occasionally with a reverse component. This is particularly evident in the dynamic analysis using the Multiple Inverse Method, where a secondary cluster of subhorizontal σ_1 is evident (Fig. 11C). In the areas of Luoboling, Zijinshan and Dajigang, strike-slip/reverse movements occurred later than the predominant normal/strike-slip movements, based on cross-cutting relationships and the presence of horizontal mineral fibres overprinting oblique fibres on individual fault surfaces. However, in many cases both sets of faults were observed containing the same syn-tectonic hydrothermal minerals: quartz in porphyry-style veins with sericitic haloes in Luoboling, and dickite in Zijinshan (Fig. 6D) and Dajigang. This indicates that faults were active with different kinematics during separate pulses of hydrothermal fluid circulation but within the duration of a single alteration event (sericitic alteration in Luoboling, advanced argillic alteration in Zijinshan and Dajigang). This is consistent with strike-slip reactivations being short-lived and probably related to local, transient changes in the stress state, rather than variations in the far-field stress regime.

A different situation is apparent in the volcano-sedimentary rocks of the Shimaoshan Group, where the areas of Yueyang, Bitian and Gushibei are located (Fig. 12). In these areas a prominent cluster of subhorizontal σ_1 was produced by the dynamic analysis (Fig. 12C). Most of the strike-slip faults contain calcite mineral fibres, and there is evidence that the strike-slip reactivation occurred after major normal movements on the same faults (Fig. 6B). This implies that strike-slip reactivation in these areas occurred late in the geologic history, after the opening of the Cretaceous volcano-tectonic basins and the accumulation of at least part of the volcano-sedimentary pile. Considering that the volcanic rocks have U-Pb ages of 110 to 99 Ma (Jiang et al., 2013, 2015), it is possible that the strike-slip reactivation of the faults in the Shimaoshan Group occurred during the compressive event postulated by Charvet et al. (1994), dated at ~100 Ma and responsible for the presence of unconformities between different segments of the Cretaceous volcano-sedimentary sequence.

In some areas (e.g., Dajigang, Fig. 14B; Zijinshan, Fig. 14C), the calculated principal stresses deviate from their expected horizontal or vertical attitude. This may be explained by late, post-mineralization block rotations of 20 to 30 degrees affecting some of the rocks of the area. Block rotation is very likely in the environment of extensional deformation predominant during and after mineralization in the Zijinshan district, associated with the activity of lystric or non-planar normal faults. However, evidence available suggest that these block rotations are a local effect of specific lystric faults, not a large-scale rotation affecting the entire Zijinshan district. Evidence against large-scale block rotation include the symmetry and similar dip angle of SW- and NE-dipping faults (Fig. 5), suggesting that they correspond to the primary dips of a conjugate set of trans-tensional faults. Strata are dipping at 10-20 degrees in the Cretaceous volcanic basins, and show no evidence for major tilting after deposition. This in turn suggests that the low to moderate dip angle of the tectonic-hydrothermal breccias emplaced in the volcanic rocks is close to their primary dip.

The existence of local post-mineral rotations suggested by deviations of the calculated principal stresses in mineralized areas, implies that at least some normal faults were still active after hydrothermal activity. This is demonstrated by drill holes in the Yueyang area. The core from hole ZK 6903 shows a fault contact between a polymict volcano-sedimentary sequence in the hanging wall and porphyritic, plagioclase- and hornblende-bearing lava flows in the foot wall. The fault was intersected at a depth of 266 m and at an angle of 50° to the core axis. The lava flows in the foot wall are cross-cut by hydrothermal veins and breccias that are truncated by the fault contact and are not present in the volcaniclastic rocks. It is likely that hydrothermal systems elsewhere in the district have also been affected by similar late-stage normal faulting. However, the absence of evidence for large-scale post-mineral rotations suggests that kilometre-scale segmentations of the deposits are unlikely.

Exploration implications

The results of this work suggest that the NW-striking faults are the most penetrative fault system in the district, and the more favourably oriented for opening under the stress regime that prevailed during mineralization. They should be considered as a highly valuable exploration guide for new targets in the area, in particular when they intersect NE-trending faults.

Based on this criterion and on the current knowledge of the distribution of alteration and mineralization in the district, the area is considered to have significant exploration potential at depth, particularly for intermediate-sulfidation epithermal and porphyry Cu-Mo deposits. Of particular interest are the inferred deep sources of known high-sulfidation epithermal mineralization. As an example, Figure 5 highlights two areas considered to have significant exploration potential for porphyry-style mineralization. They are the inferred sources of outcropping, fault-controlled hydrothermal breccias associated with high-sulfidation epithermal alteration and mineralization. One of the highlighted areas is located at depth between Zijinshan and Luoboling. The area is the inferred source of the fault-controlled hydrothermal breccias and veins of Zijinshan (Fig. 5), and would be located very close to the deep part of the known porphyry-style mineralization of Luoboling (Fig. 5). It is possible that Zijinshan and Luoboling are surface expressions of the same system at depth. Whether that is the case, or if they instead have proximal but discrete fluid sources, there is still considerable exploration potential for porphyry-style mineralization at depth to the SW of the known mineralization at Luoboling.

The second area highlighted has potential for porphyry-style mineralization at what is inferred to be the source of the fault-controlled hydrothermal breccias and veins in the Dajigang-Sanqingting area. Outcrops in this area show abundant evidence of alteration and mineralization typical of the high-sulfidation epithermal environment (quartz-dickite-pyrite-Au). It includes the largest complex of tectonic-hydrothermal breccias observed in the district outside of the Zijinshan deposit (Fig. 8A). The area is of interest both for the exploration of HS epithermal mineralization close to the surface, and for porphyry-style mineralization at depth (Fig. 5). This potential has not been tested with drilling. Because of the moderate dip of the NW-striking faults and breccias, the porphyry target, which corresponds to the source of the hydrothermal fluids responsible for the alteration and mineralization observed at Dajigang-Sanqingting, should be located to the SW of the surface expression of the hydrothermal system (Fig. 5). This target might also be associated with intermediate-sulfidation veins emplaced at structurally-favourable positions in the volcanic rocks of the Shimaoshan Group to the SW (Fig. 5).

Giant porphyry deposits, in particular porphyry Cu-Mo deposits, typically form in convergent magmatic arcs under compressional to transpressional conditions, commonly during the last stages of continental-scale events of crustal thickening, shortening, uplift and exhumation (e.g. Cooke et al., 2005; Sillitoe, 2010; Piquer et al., 2015, 2016). However, this is not the case in the Zijinshan district, where hydrothermal minerals related with porphyry Cu-Mo and high-sulfidation epithermal Cu-Au deposits precipitated in normal faults under an extensional stress regime (sub-vertical σ_1). This situation demonstrates that while giant porphyry Cu-Mo deposits might be exclusively found emplaced in thickened continental crust under compressional to transpressional regimes, smaller porphyry Cu-Mo deposits (and large high-sulfidation epithermal Cu-Au deposits) can form in magmatic arcs associated with a retreating trench and an extensional continental margin, such as the Late Yanshanian arc of SE China. McCuaig and Hronsky (2014) proposed three transient geodynamic settings favourable for the formation of mineral systems: anomalous compression, initial stages of extension and switches in the prevailing stress field. As mentioned before, the first of these three settings is the most favourable for the formation of giant porphyry-epithermal systems, but Zijinshan appears to be a rare case of porphyry-style and epithermal mineralization under the second and third scenarios: initial stages of extension after a major switch from compression to extension, marking the transition between the Early and Late Yanshanian. This implies that the exploration potential for porphyry Cu-Mo deposits of other extensional arcs should be re-evaluated, in particular when the early stages of syn-extensional magmatism ascended through previously-thickened continental crust.

Conclusions

The structural geology of the Zijinshan district is dominated by several NW-striking fault systems that dip at moderate angles (40-50°) to the NE and SW. They are the largest, most continuous fault systems in the district, with the widest damage zones. Statistically, they are the predominant fault population, and they played a first-order role controlling the emplacement of hydrothermal veins and breccias in different mineralized centres. During mineralization, the NW-striking faults were active as conjugate sets of oblique normal/strike-slip faults, as evidenced by syn-tectonic hydrothermal minerals. A small number of NW-striking faults show evidence of strike-slip reactivation.

NE-striking faults also played a major role in the structural evolution of the district. They dip at higher angles than the NW-striking faults, and are parallel to the axis of a regional-scale anticline, the core of which was intruded by Jurassic plutons. During mineralization, some NE-striking faults also controlled the emplacement of veins and breccias, although to a much lesser extent than the NW-striking faults. Syn-tectonic mineral fibres indicate predominantly dextral strike-slip movements for this group of faults.

The similarities between the district- and continental-scale structural architecture, both dominated by NW- and NE-striking faults, suggest that the fault systems present in the district correspond to the local expressions of continental-scale, long-lived structural systems.

Kinematic and dynamic analyses of fault-slip data shows that the predominant tectonic regime during mineralization was extensional, with subvertical σ_1 and σ_3 trending on average to the NNE. This implies that the NW-striking faults were the most favourably oriented for opening under the tectonic regime prevalent during mineralization. Secondary clusters of subhorizontal σ_1 indicate fault reactivation events under a strike-slip regime. Most of them appear to have been very short-lived and related to local tectonics, with the exception of a more well-developed fault reactivation event observed in rocks of the Shimaoshan Group, which could be related to a contractional event occurring at ~100 Ma that was recognized in the area by previous workers.

Several new exploration targets can be proposed in the district based on structural criteria and the ever-growing geological knowledge about the hydrothermal systems of the district. There is still a considerable untested exploration potential in the district, mainly for porphyries (including the sources of known high-sulfidation systems) and intermediate-sulfidation deposits.

The syn-extensional character of porphyry- and epithermal-style mineralization in the Zijinshan district show that, although the formation of porphyry Cu-Mo systems is commonly favoured by compressive to transpressive tectonic regimes, exceptions to the rule exist and at least medium-sized porphyry Cu-Mo systems (and large high- to intermediate-sulfidation epithermal systems) can be found in extensional volcanic arcs with a retreating trench. This has important implications for the exploration of other extensional arcs, which are commonly considered non-prospective for porphyry Cu-Mo deposits.

Acknowledgments

The Zijin Mining Group Co. is acknowledged for providing logistical support for fieldwork and for allowing the publication of this work.

REFERENCES

Allmendinger, R. W., Cardozo, N., and Fisher, D. M., 2012, Structural Geology algorithms: vectors and tensors: New York, Cambridge University Press, 302 p.

Bott, M. H. P., 1959, The mechanics of oblique slip faulting: Geological Magazine, v. 96, p. 109-117.

Charvet, J., Lapierre, H., and Yu, Y., 1994, Geodynamic significance of the Mesozoic volcanism of southeastern China: Journal of Southeast Asian Earth Sciences, v. 9, p. 387-396.

Chen, J., Cooke, D. R., Zhang, L., White, N. C., Chen, H., and Qi, J., 2015, Hydrothermal alteration, mineralization and breccias at the Zijinshan high sulfidation Cu-Au deposit, Fujian Province, China: SGA Biennial Meeting, 13th, Nancy, France, 24-27 August 2015, Abstracts.

Cooke, D. R., Hollings, P., and Walshe, J., 2005, Giant porphyry deposits: characteristics, distribution, and tectonic control: Economic Geology, v. 100, p. 801-818.

Feng, Z.Z., 1993, Mesozoic volcanism and tectonic environment in Fujian Province: Regional geology of China, v. 12, p. 311-316 (in Chinese).

Jiang, S.-H., Liang, Q.-L., Bagas, L., Wang, S.-H., Nie, F.-J., and Liu, Y.-F., 2013, Geodynamic setting of the Zijinshan porphyry–epithermal Cu–Au–Mo–Ag ore system, SW Fujian Province, China: Constraints from the geochronology and geochemistry of the igneous rocks: Ore Geology Reviews, v. 53, p. 287-305.

Jiang, S.-H., Bagas, L., and Liang, Q.-L., 2015, New insights into the petrogenesis of volcanic rocks in the Shanghang Basin in the Fujian Province, China: Journal of Asian Earth Sciences, v. 105, p. 48-67.

Lai, X., and Qi, J., 2014, The regularity of structural controls on ore mineralization in the Luoboling porphyry Cu-Mo deposit, Shanghang, Fujian: Acta Geologica Sinica, v. 88, p. 1904-1916.

Li, B., and Jiang, S.-Y., 2014, Geochronology and geochemistry of Cretaceous Nanshanping alkaline rocks from the Zijinshan district in Fujian Province, South China: Implications for crust–mantle interaction and lithospheric extension: Journal of Asian Earth Sciences, v. 93, p. 253-274.

Li, B., and Jiang, S.-Y., 2015, A subduction-related metasomatically enriched mantle origin for the Luoboling and Zhongliao Cretaceous granitoids from South China: Implications for magma evolution and Cu-Mo mineralization: International Geology Review, v. 57, p. 1239-1266.

Liu, X., and Hua, R., 2005, $^{40}Ar/^{39}Ar$ dating of adularia from the Bitian gold–silver–copper deposit, Fujian Province: Geology Reviews, v. 51, p. 151-155.

Mao, J., Li, X., White, N. C., Zhao, C., Zhang, Z., Wang, Y., and Hu, H., 2007, Types, characteristics, and geodynamic settings of Mesozoic epithermal gold deposits in Eastern China: Resource Geology, v. 57, p. 435-454.

Mao, J., Cheng, Y., Chen, M., and Pirajno, F., 2013, Major types and time–space distribution of Mesozoic ore deposits in South China and their geodynamic settings: Mineralium Deposita, v. 48, p. 267-294.

Marrett, R., and Allmendinger, R. W., 1990, Kinematic analysis of fault-slip data: Journal of Structural Geology, v. 12, p. 973-986.

McCuaig, T. C., and Hronsky, J. M. A., 2014, The mineral system concept: the key to exploration targeting: Society of Economic Geologists Special Publication 18, p. 153-175.

Petit, J. P., 1987, Criteria for the sense of movement on fault surfaces in brittle rocks: Journal of Structural Geology, v. 9, p. 597-608.

Piquer, J., Skarmeta, J., and Cooke, D.R., 2015, Structural evolution of the Rio Blanco-Los Bronces District, Andes of Central Chile: controls on stratigraphy, magmatism and mineralization: Economic Geology, v. 110, p. 1995-2023.

Piquer, J., Berry, R.F., Scott, R.J., and Cooke, D.R., 2016, Arc-oblique fault systems: their role in the Cenozoic structural evolution and metallogenesis of the Andes of central Chile: Journal of Structural Geology, v. 89, p. 101-117.

Pirajno, F., and Bagas, L., 2002, Gold and silver metallogeny of the South China Fold Belt: a consequence of multiple mineralizing events?: Ore Geology Reviews, v. 20, p. 109-126.

Sillitoe, R. H., 2010, Porphyry copper systems. Economic Geology, v. 105, p. 3-41.

So, C.-S., Zhang, D.-Q., Yun, S.-T., and Li, D.-X., 1998, Alteration-Mineralization zoning and fluid inclusions of the high sulfidation epithermal Cu-Au mineralization at Zijinshan, Fujian Province, China: Economic Geology, v. 93, p. 961-980.

Wallace, R. E., 1951, Geometry of shearing stress and relation of faulting: Journal of Geology, v. 59, p. 118-130.

Yamaji, A., 2000, The multiple inverse method: a new technique to separate stresses from heterogeneous fault-slip data: Journal of Structural Geology, v. 22, p. 441-452.

Zaw, K., Peters, S. G., Cromie, P., Burrett, C., and Hou, Z., 2007, Nature, diversity of deposit types and metallogenic relations of South China: Ore Geology Reviews, v. 31, p. 3-47.

Zhang, D., Li, D., Feng, C., and Dong, Y., 2001, The temporal and spatial framework of the Mesozoic magmatic system in Zijinshan area and its geological significance: Acta Geologica Sinica, v. 22, p. 403-408.

Zhang, D.Q., Feng, C.Y., Li, D.X., She, H.Q., and Dong, Y.J., 2003, ^{40}Ar–^{39}Ar dating of adularia from Bitian sericite-adularia type epithermal Ag–Au deposit in Fujian Province and its geological significance: Mineral Deposits, v. 22, p. 360–364.

Zhong, J., Chen, Y.-J., Pirajno, F., Chen, J., Li, J., Qi, J.-P., and Li, N., 2014, Geology, geochronology, fluid inclusion and H–O isotope geochemistry of the Luoboling porphyry Cu–Mo deposit, Zijinshan Orefield, Fujian Province, China: Ore Geology Reviews, v. 57, p. 61-77.

Zhou, X., and Li, W., 2000, Origin of Late Mesozoic igneous rocks in Southeastern China: implications for lithosphere subduction and underplating of mafic magmas: Tectonophysics, v. 326, p. 269-287.

Zhou, T., Goldfarb, R. J., and Phillips, G. N., 2002, Tectonics and distribution of gold deposits in China—an overview: Mineralium Deposita, v. 37, p. 249-282.

Zhou, X., Sun, T., Shen, W., Shu, L., and Niu, Y., 2006, Petrogenesis of Mesozoic granitoids and volcanic rocks in South China: A response to tectonic evolution: Episodes, v. 29, p. 26-33.

FIGURE CAPTIONS

Figure 1. A. Location of the Zijinshan district in Fujian Province, China. B. Distribution of mines, exploration prospects and villages of the Zijinshan district, showing also the location of the town of Shanghang.

Figure 2. A. Main tectonic blocks and fault systems of SE China. The Yangtze Craton and the Cathaysia block together constitute the South China Block. Modified from Zaw et al. (2007) and Pirajno and Bagas (2002). B. Main fault systems and volcanic basins in the region surrounding the Zijinshan district, south-western Fujian Province. SYF = Shanghang-Yunxiao Fault; XA = Xuanhe Anticlinorium. Modified from Jiang et al. (2013).

Figure 3. Distribution of structural stations (black triangles) in the Zijinshan district, showing the areas into which the district was subdivided for structural analysis. The Ting and Jiuxian rivers are shown for reference.

Figure 4. Simplified geological map of the study area, based on this work and the unpublished geological map of the Zijin Mining Group Co. F 1-1, F 1-4, F 2-1 and F 2-10 refer to some of the main faults identified in previous publications and are labelled here for correlation. The trace of the cross-section of Fig. 5 is shown in blue.

Figure 5. Simplified long section of the Zijinshan district. See Figure 4 for legend and cross-section location. Faults and tectonic-hydrothermal breccias are shown in blue. Black lines represent bedding.

Figure 6. Examples of steps in syn-tectonic hydrothermal mineral fibres. Arrows indicate sense of movement of the missing block. UTM coordinates in meters. A. Steps in calcite fibres in the hanging wall of a dextral-normal fault (437424mE, 2783186mN, 205m a.s.l). B. Steps in calcite fibres in the footwall of a sinistral-reverse fault (441272mE, 2778348mN, 271m a.s.l). This fault juxtaposes Carboniferous limestones in the hanging wall and Cretaceous andesitic lava flows in the footwall. The stratigraphic correlation indicates a major normal displacement, but the steps in calcite show that the fault was later reactivated in sinistral-reverse mode. C. Steps in calcite fibres in the hanging wall of a dextral-normal fault

(437424mE, 2783186mN, 205m a.s.l). D. Steps in dickite fibres in the footwall of a sinistral-reverse fault (439922mE, 2786677mN, 586m a.s.l). E. Steps in hematite-quartz in the footwall of a normal-sinistral fault associated with ~15 cm of tectonic breccia and fault gouge (437022mE, 2785792mN, 217m a.s.l). F. Steps in hematite-dickite-kaolinite in the footwall of a dextral-normal fault (438211mE, 2784190mN, 208m a.s.l). G. Steps in dickite-hematite in the footwall of a dextral-normal fault (438493mE, 2783843mN, 346m a.s.l).

Figure 7. Structural control on the geometry of hydrothermal alteration zones. A. Quartz-dickite alteration zone with disseminated pyrite (dashed yellow line represents the alteration front) around a NW-striking, subvertical fault. Luoboling project (444528mE, 2789549mN). B. Quartz-argillic alteration zone with abundant jarosite and goethite. The alteration front defines a NW-striking plane dipping to the SW, parallel to the main fault trend cropping out in the area. Dajigang project (438228mE, 2784107mN). C. Area of strong quartz-dickite alteration with goethite, jarosite and Cu oxides, surrounding NW-striking, NE-dipping hydrothermal breccias, and bounded by faults with the same orientation. Zijinshan open pit (440027mE, 2786653mN).

Figure 8. A. Set of NW-striking tectonic-hydrothermal breccias, dipping at moderate angles to the SW. A NW-striking, NE-dipping conjugate faults is also present. Dajigang area (438468mE, 2783801mN). B. Multiple generations of breccias and veins in the Zijinshan deposit. Pyrite-covellite veins are truncated and displaced by younger, pyrite- and covellite-rich tectonic-hydrothermal breccias (the largest of them labelled as T-H breccia) and by a late pebble dike which cross-cut both the veins and the breccias. The yellow arrows highlight the position of different segments of a single truncated pyrite vein. The sense of movement along the tectonic breccias and the pebble dike is oblique normal-sinistral (440521mE, 2786922mN).

Figure 9. NE-trending, subvertical dacitic dike with quartz phenocrysts and foliated margins. The dike is emplaced along a NE-striking fault. Bitian area (437410mE, 2783140mN).

Figure 10. Syn-tectonic sedimentary and pyroclastic deposits of the Cretaceous Shimaoshan Group. Thick yellow lines highlight the variations in thickness of a given stratigraphic package. A. Growth strata in a sequence of volcanogenic sedimentary deposits and possible distal pyroclastic deposits. The sequence contains almost exclusively reworked lithic fragments. Yueyang area (435891mE, 2784588mN). B. NW-striking, SW-dipping normal fault located adjacent to the NE of the sequence shown at (A). The fault juxtaposes different volcano-sedimentary packages. C. Growth strata in a sequence of rhyolitic pyroclastic deposits, rich in quartz, K-feldspar and plagioclase crystal fragments and volcanic lithics. Bitian area (436358mE, 2782581mN).

Figure 11. Results of the analysis of fault plane data for the Zijinshan district. A. Rose diagram for the dip directions of the 548 fault planes contained in the database. B. Results of the kinematic analysis of fault-slip data; lower-hemisphere, equal-area projection. The stereoplot shows the pressure and tension axes for each fault plane as blue and red dots respectively, together with the average kinematic axes (1 = shortening, 2 = intermediate, 3 =

stretching). C. Results of the dynamic analysis of fault-slip data; lower-hemisphere, equal-area projections. The two stereoplots show the calculated orientations of σ_1 and σ_3 for subgroups of fault-slip data using the Multiple Inverse Method.

Figure 12. A. Rose diagrams for the dip direction of faults in the Yueyang, Bitian and Gushibei areas. B and C. Results of the kinematic and dynamic analysis, respectively, for the combined areas of Yueyang, Bitian and Gushibei. Stereoplots and legend as in Fig. 11.

Figure 13. A. NW-striking, subvertical fault in the Gushibei area. The fault puts in contact andesitic lava flows to the NE (dark colour, left) with eutaxitic ignimbrites to the SW (light colour, right; 440857mE, 2779031mN). B. NW-striking tectonic-hydrothermal breccia in the Dajigang area, dipping ~50°SW. These breccias have been the subject of small-scale Au mining (438468mE, 2783801mN).

Figure 14. Results of the analysis of fault plane data for the areas of A. Longjiangting and Ermiaogou; B. Dajigang and Sanqingting; C. Zijinshan open pit area; D. Luoboling and Wuziqilong. For each area, the plot to the left corresponds to a rose diagram for the dip direction of fault planes. The next three plots are all lower hemisphere, equal-area projections. The first panel (centre-left) shows the P and T axes for each fault plane together with the average kinematic axes, while the two stereoplots to the right show the calculated orientations of σ_1 and σ_3 for subgroups of fault-slip data using the Multiple Inverse Method. Colour legend in the stereoplots and numbering of the kinematic axes as in Fig. 11.

Figure 15. Major faults in the Zijinshan open pit, highlighted by yellow arrows. Both faults strike to the NW and dip moderately to the NE. View to the NW from 440027mE, 2786653mN. Picture taken on November 18, 2014.

Figure 16. NW-striking faults in the Luoboling area. A. System of en-echelon faults dipping at high angle to the NE. The faults contain syn-tectonic dickite indicating dextral-normal movement and syn-tectonic calcite indicating sinistral-normal movement (444790mE, 2789640mN). B. Central fault of a NW-striking fault system dipping 70-75°SW. The fault contains ~10 cm of tectonic breccia. The fault system is associated with strong quartz-argillic alteration, goethite-jarosite disseminations and locally quartz-pyrite ± molybdenite veins with sericitic halos ("D" veins). The veins are polydirectional but are restricted to the vicinity of the NW-striking faults. The fault planes contain abundant syn-tectonic quartz fibres which mostly indicate normal-sinistral movement, although some of them show evidence of sinistral-reverse reactivation. C. "D" vein in the vicinity of the fault system of B.

Figure 17. Results of the analysis of fault plane data for the areas to the NE and SE of Zijinshan. For each area, the plot to the left correspond to a rose diagram for the dip direction of fault planes. The stereoplot to the right shows the P and T axes for each fault plane together with the average kinematic axes. Colour legend and numbering of kinematic axes as in Fig. 11.

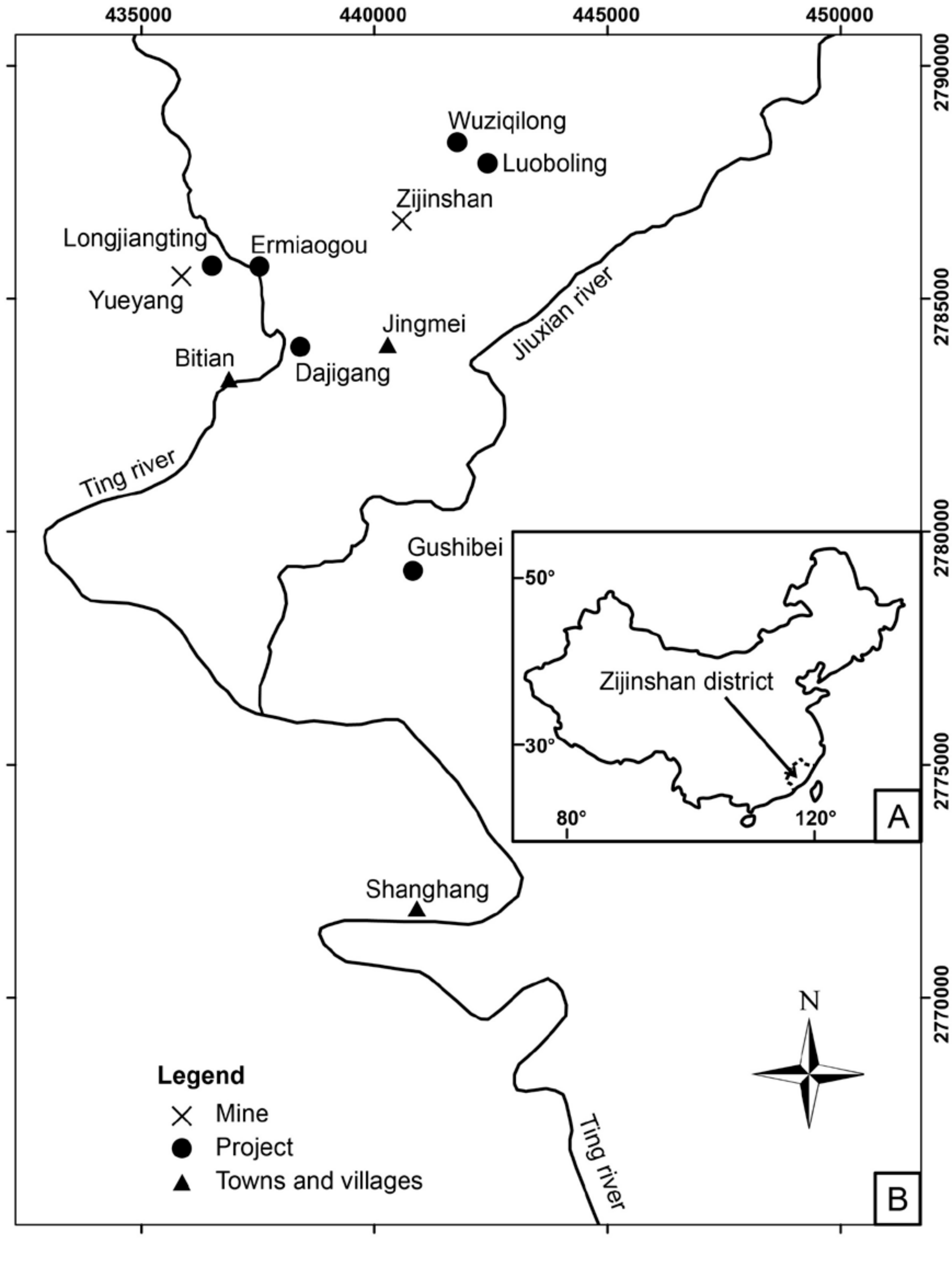

435000
440000
445000
450000
2790000
2785000
2780000
2775000
2770000
Wuziqilong
Luoboling
Zijinshan
Longjiangting
Ermiaogou
Yueyang
Jingmei
Jiuxian river
Bitian
Dajigang
Ting river
Gushibei
50°
30°
80°
120°
Zijinshan district
A
Shanghang
N
Legend
Mine
Project
Towns and villages
Ting river
B

Figure 1

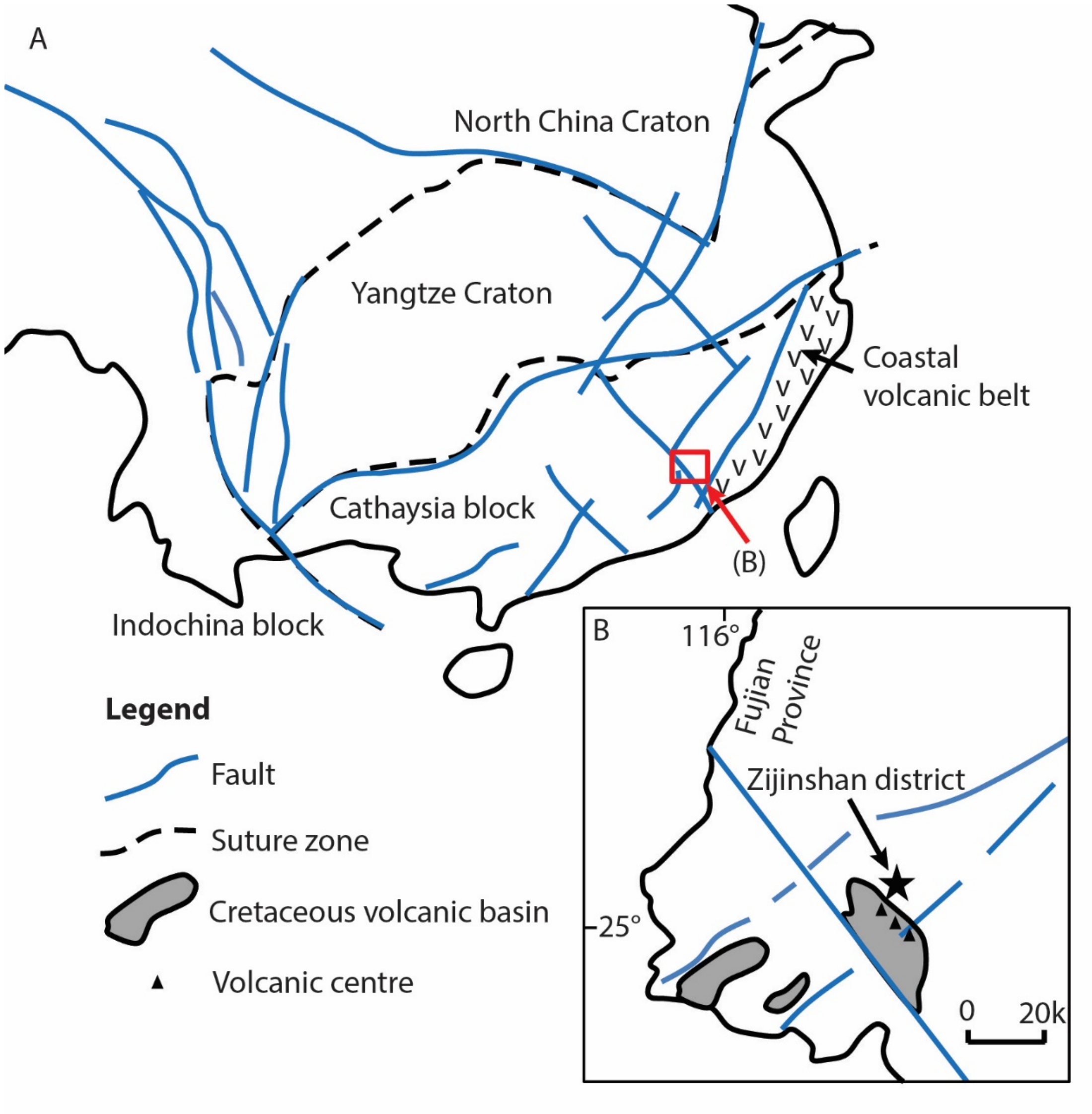
A
North China Craton
Yangtze Craton
Coastal
volcanic belt
Cathaysia block
(B)
Indochina block
Legend
Fault
Suture zone
Cretaceous volcanic basin
Volcanic centre
B
116°
Fujian
Province
Zijinshan district
25°
0
20k

Figure 2

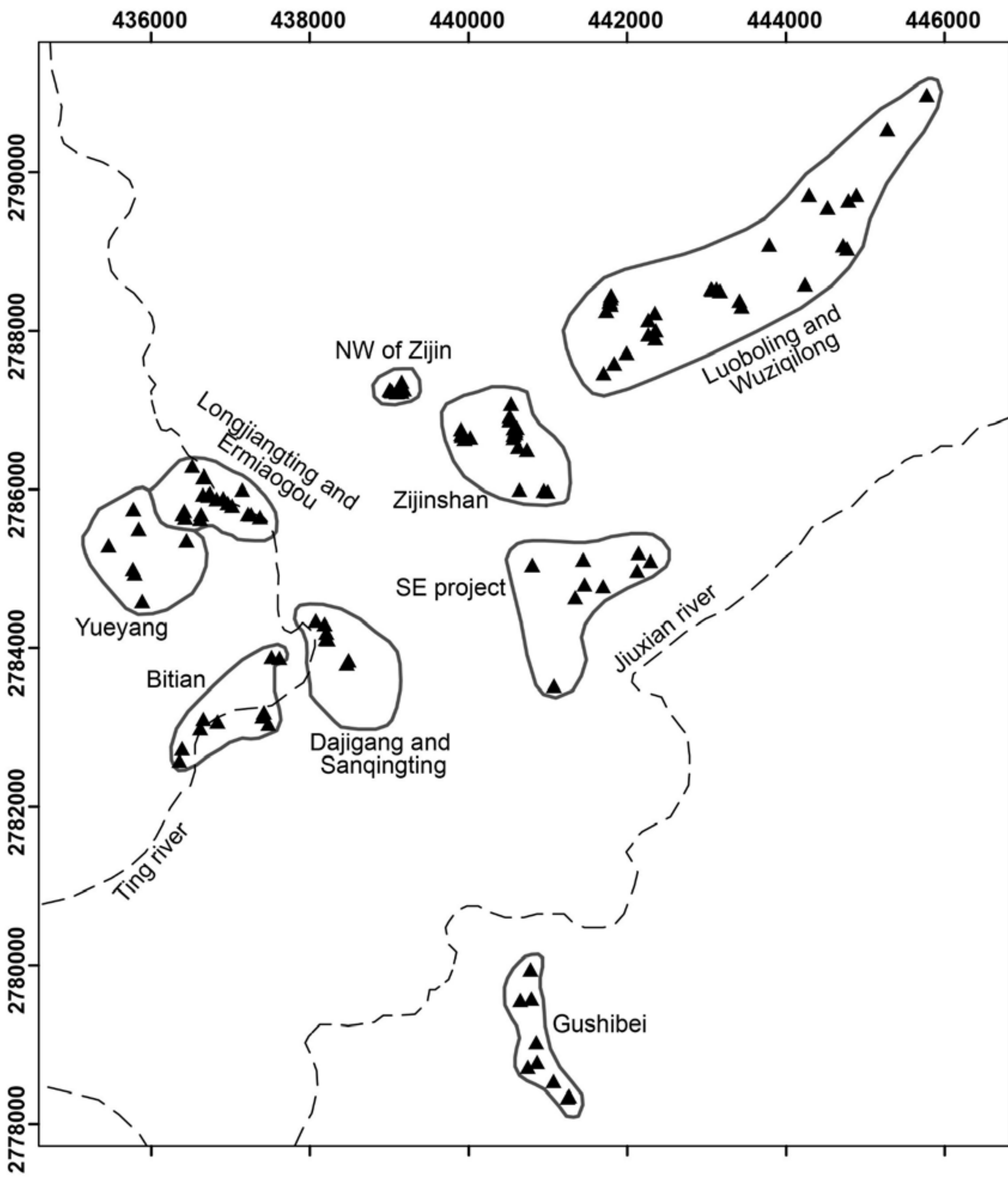
436000
438000
440000
442000
444000
446000
2790000
2788000
2786000
2784000
2782000
2780000
2778000
Luoboling and Wuziqilong
NW of Zijin
Zijinshan
Longjiangting and Ermiaogou
Yueyang
SE project
Jiuxian river
Bitian
Dajigang and Sanqingting
Ting river
Gushibei

Figure 3

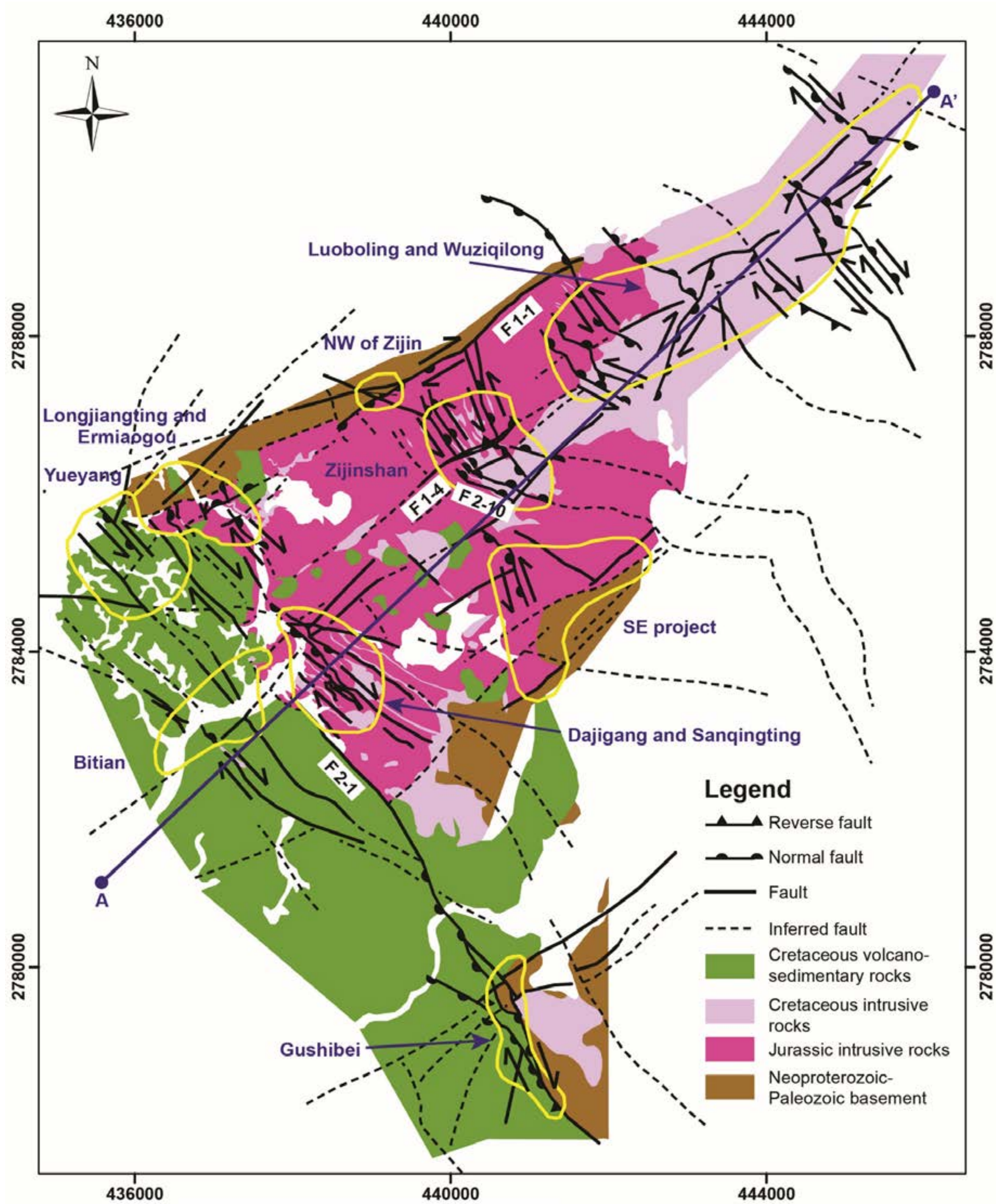
436000
440000
444000
2788000
2784000
2780000
N
A'
A
Luoboling and Wuziqilong
NW of Zijin
F1-1
Longjiangting and Ermiaogou
Yueyang
Zijinshan
F1-4
F2-10
SE project
Dajigang and Sanqingting
Bitian
F2-1
Gushibei
Legend
Reverse fault
Normal fault
Fault
Inferred fault
Cretaceous volcano-sedimentary rocks
Cretaceous intrusive rocks
Jurassic intrusive rocks
Neoproterozoic-Paleozoic basement

Figure 4

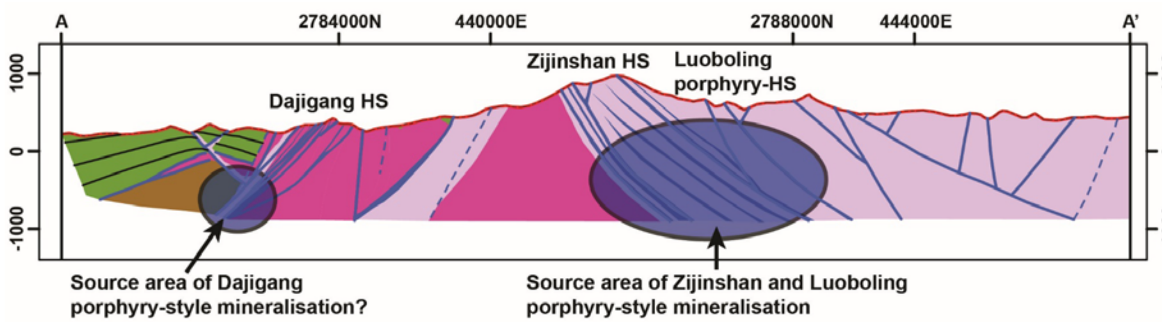
A
2784000N
440000E
2788000N
444000E
A'
1000
0
-1000
Zijinshan HS
Luoboling
porphyry-HS
Dajigang HS
Source area of Dajigang
porphyry-style mineralisation?
Source area of Zijinshan and Luoboling
porphyry-style mineralisation

Figure 5

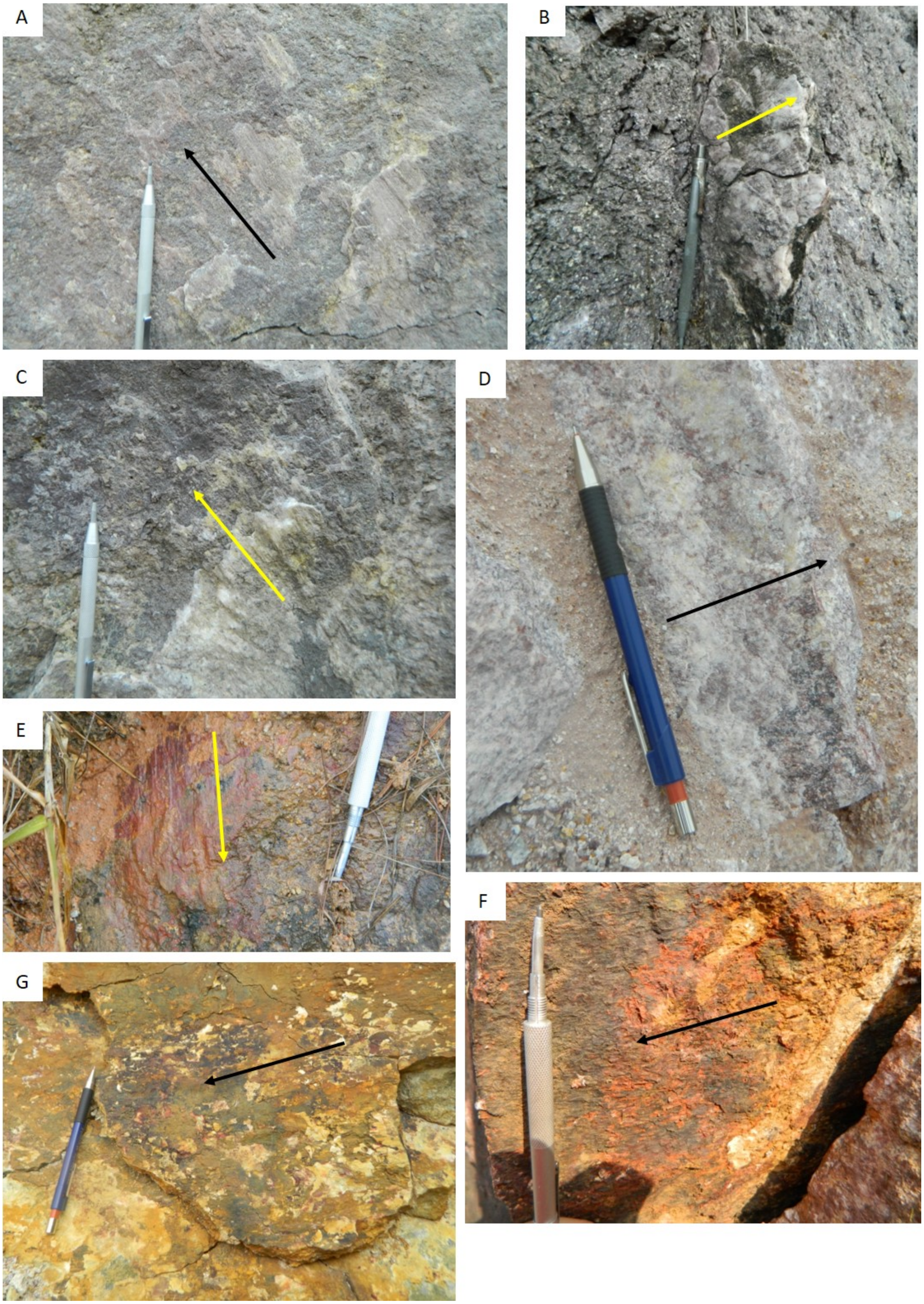

Figure 6

Figure 7

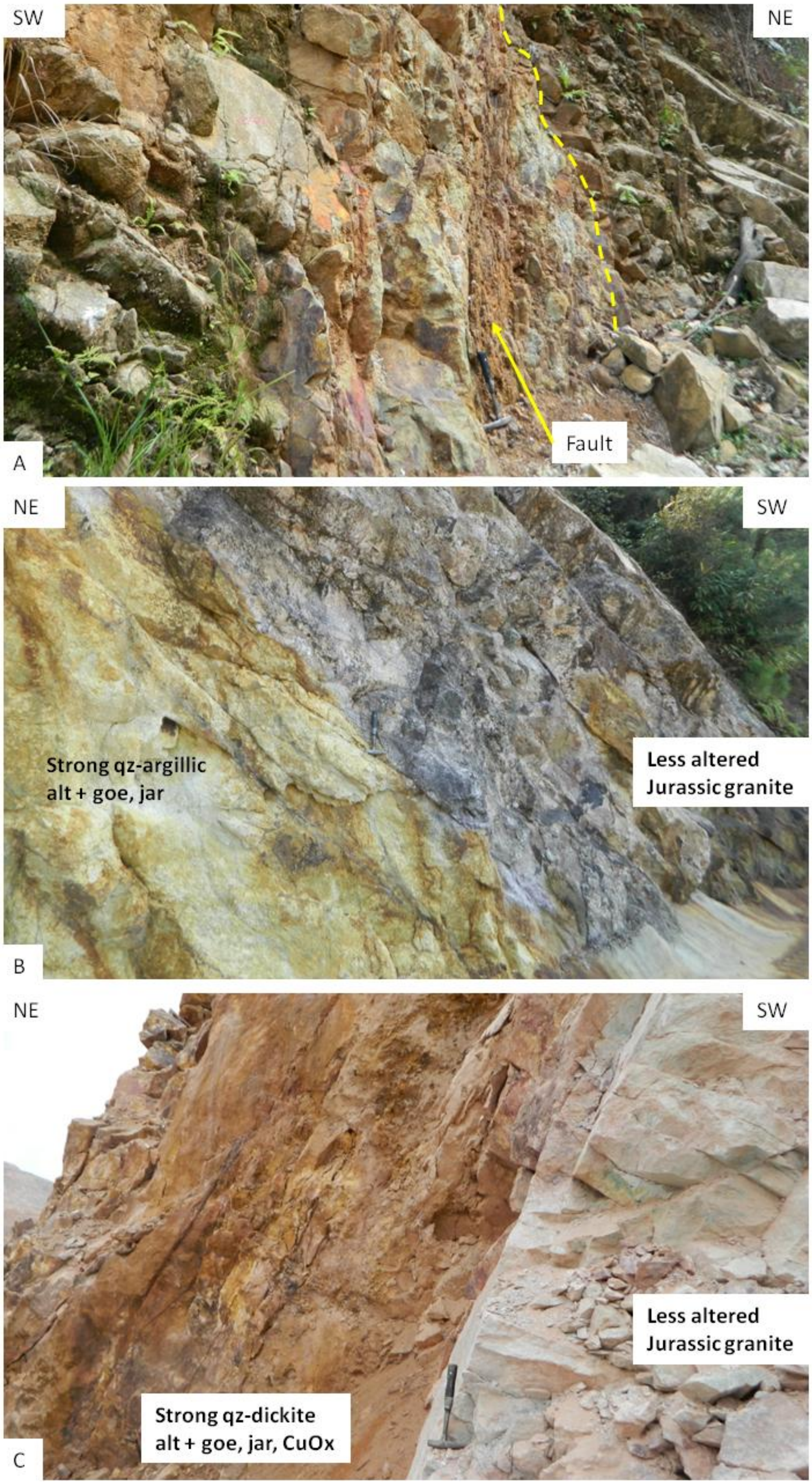
SW
NE
Fault
A
NE
SW
Strong qz-argillic
alt + goe, jar
Less altered
Jurassic granite
B
NE
SW
Less altered
Jurassic granite
Strong qz-dickite
alt + goe, jar, CuOx
C

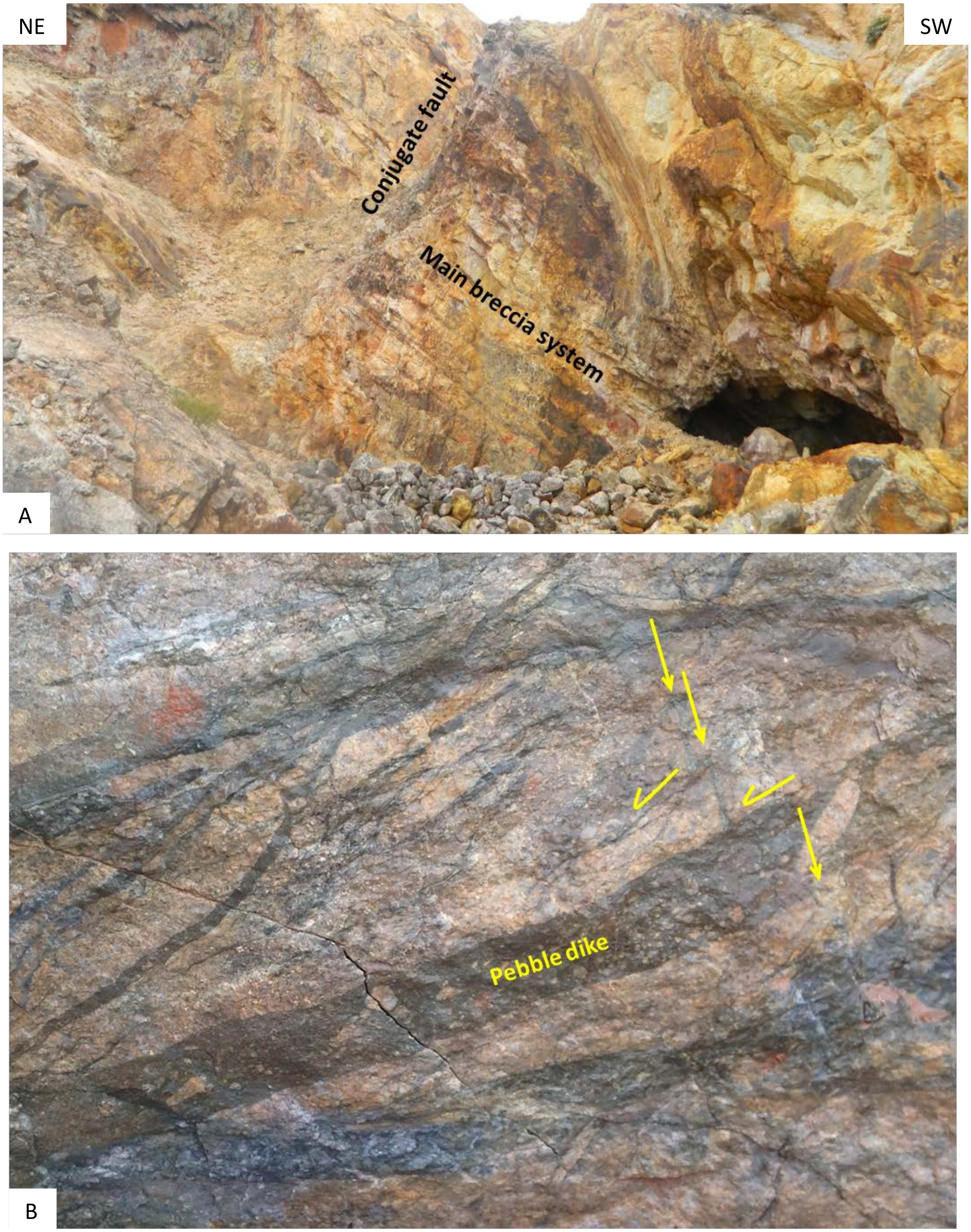

Figure 8

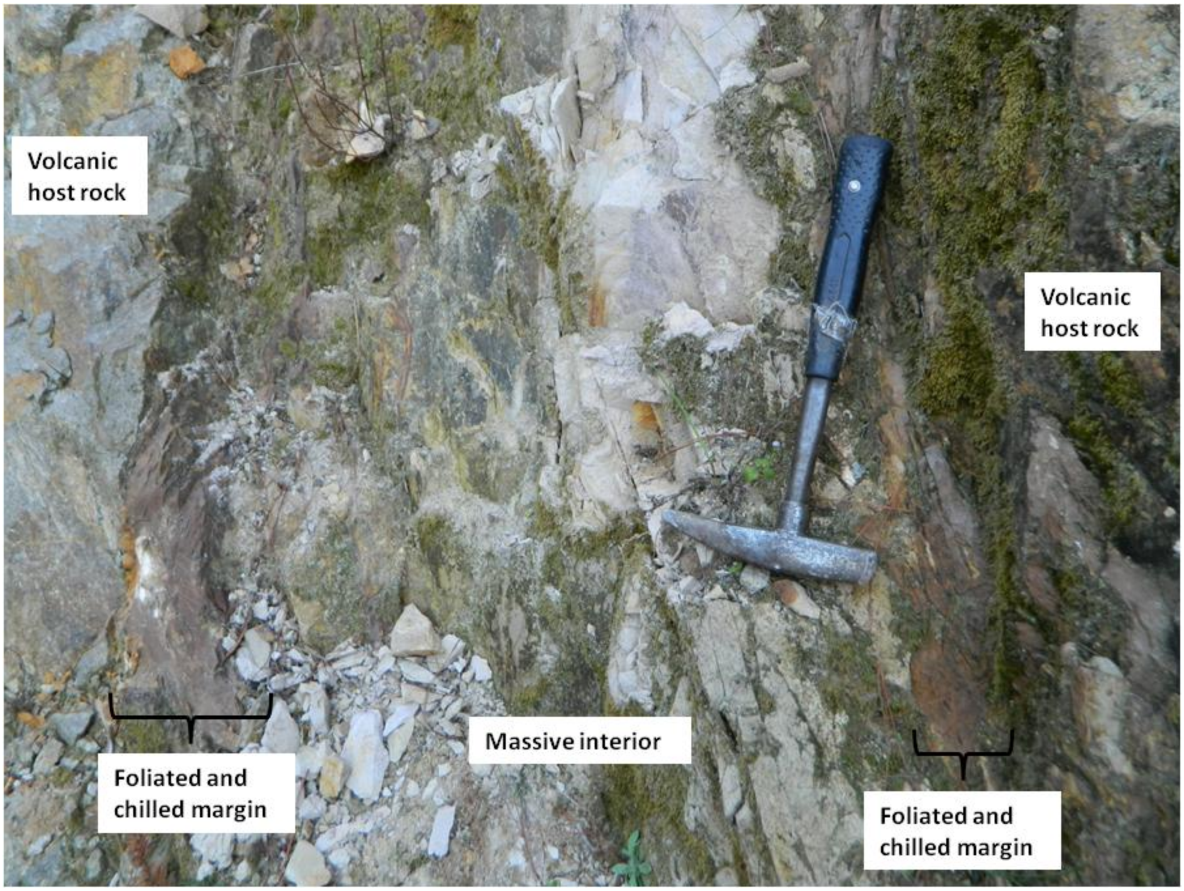
Volcanic host rock
Volcanic host rock
Massive interior
Foliated and chilled margin
Foliated and chilled margin

Figure 9

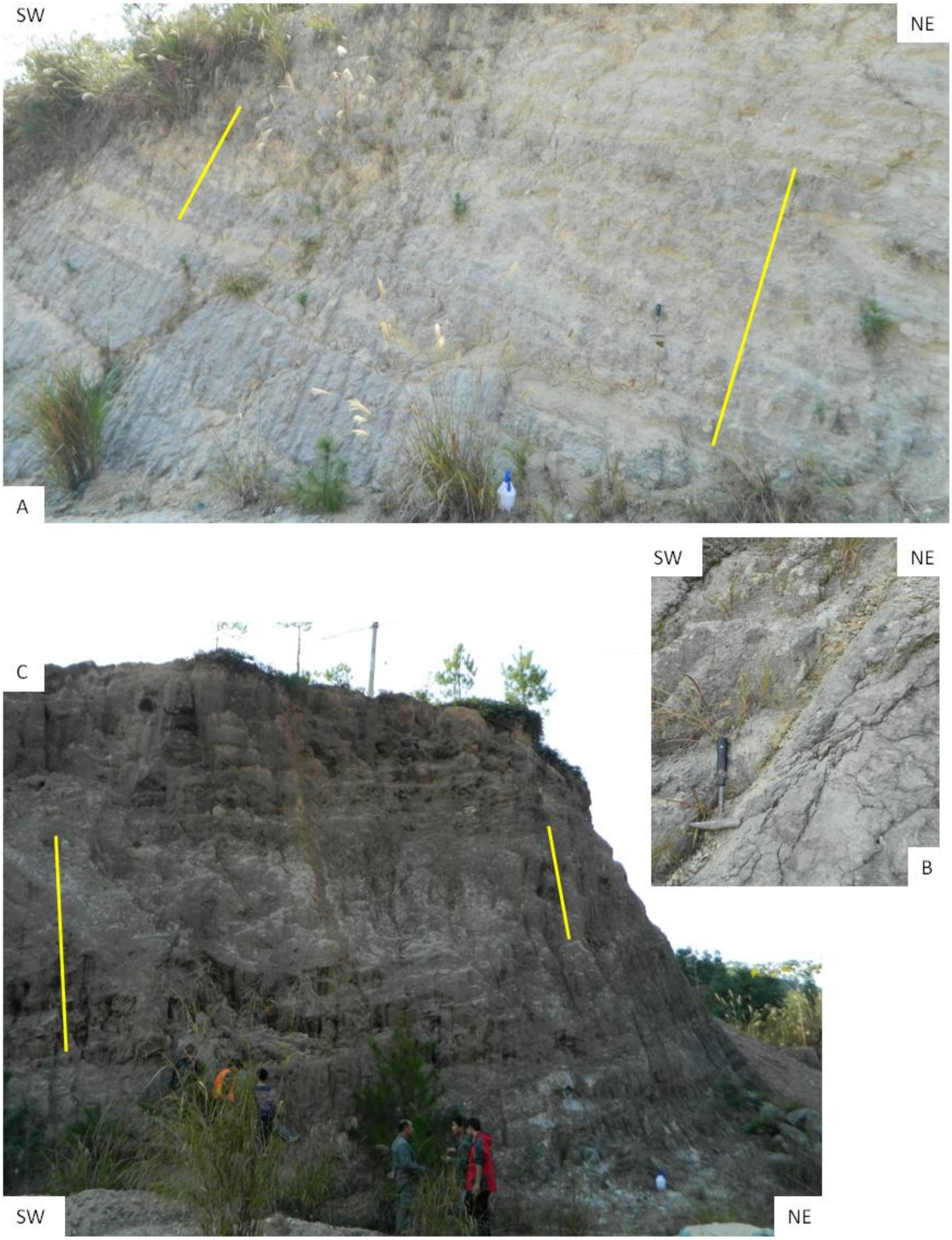

Figure 10

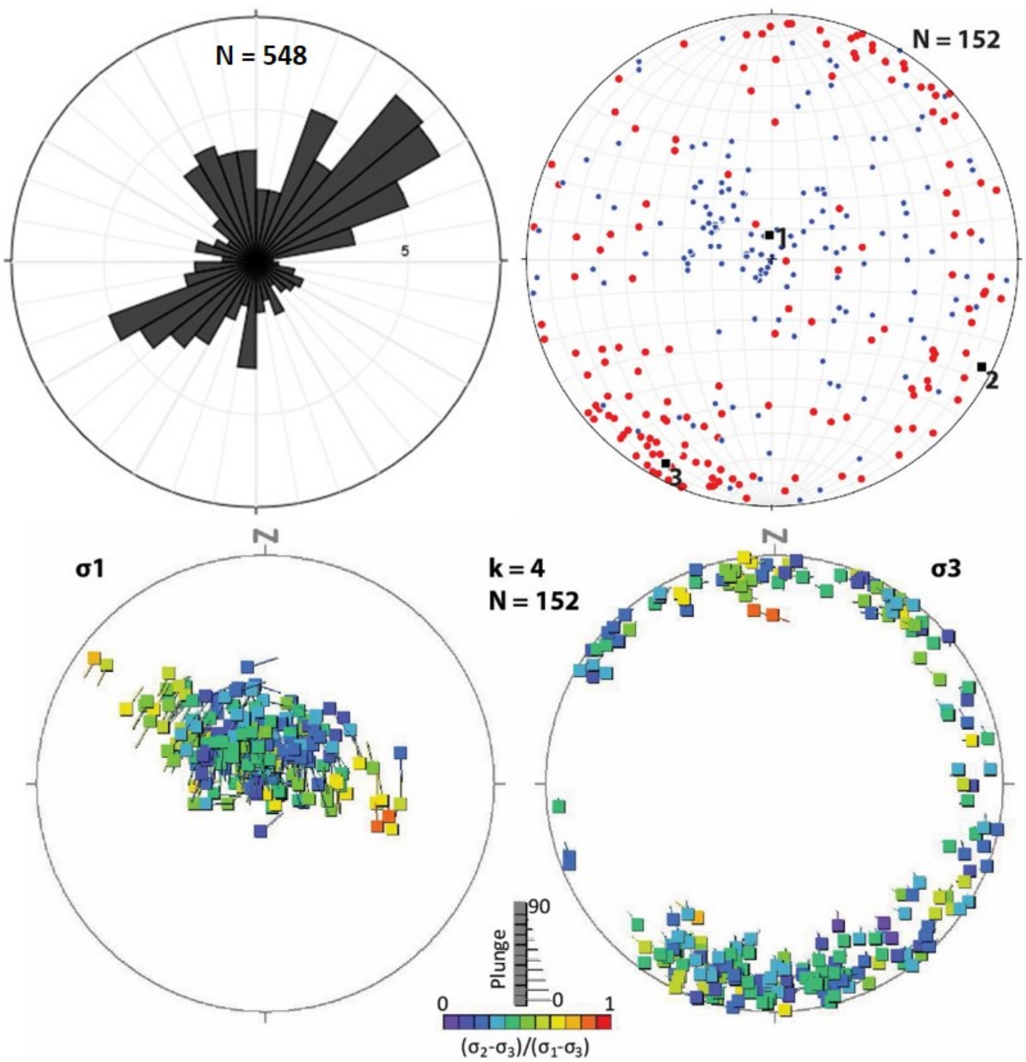

Figure 11

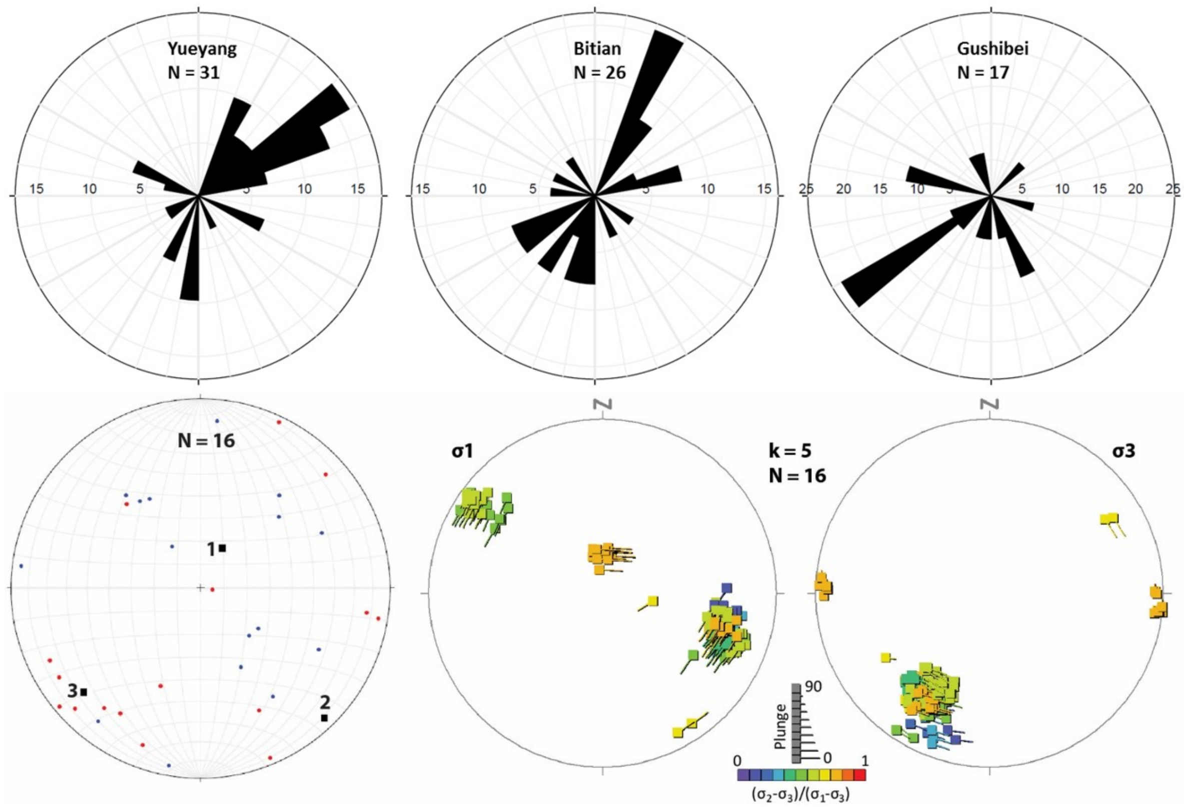
Yueyang
N = 31
Bitian
N = 26
Gushibei
N = 17
N = 16
1
2
3
σ1
k = 5
N = 16
σ3
N
Plunge
90
0
(σ2-σ3)/(σ1-σ3)

Figure 12

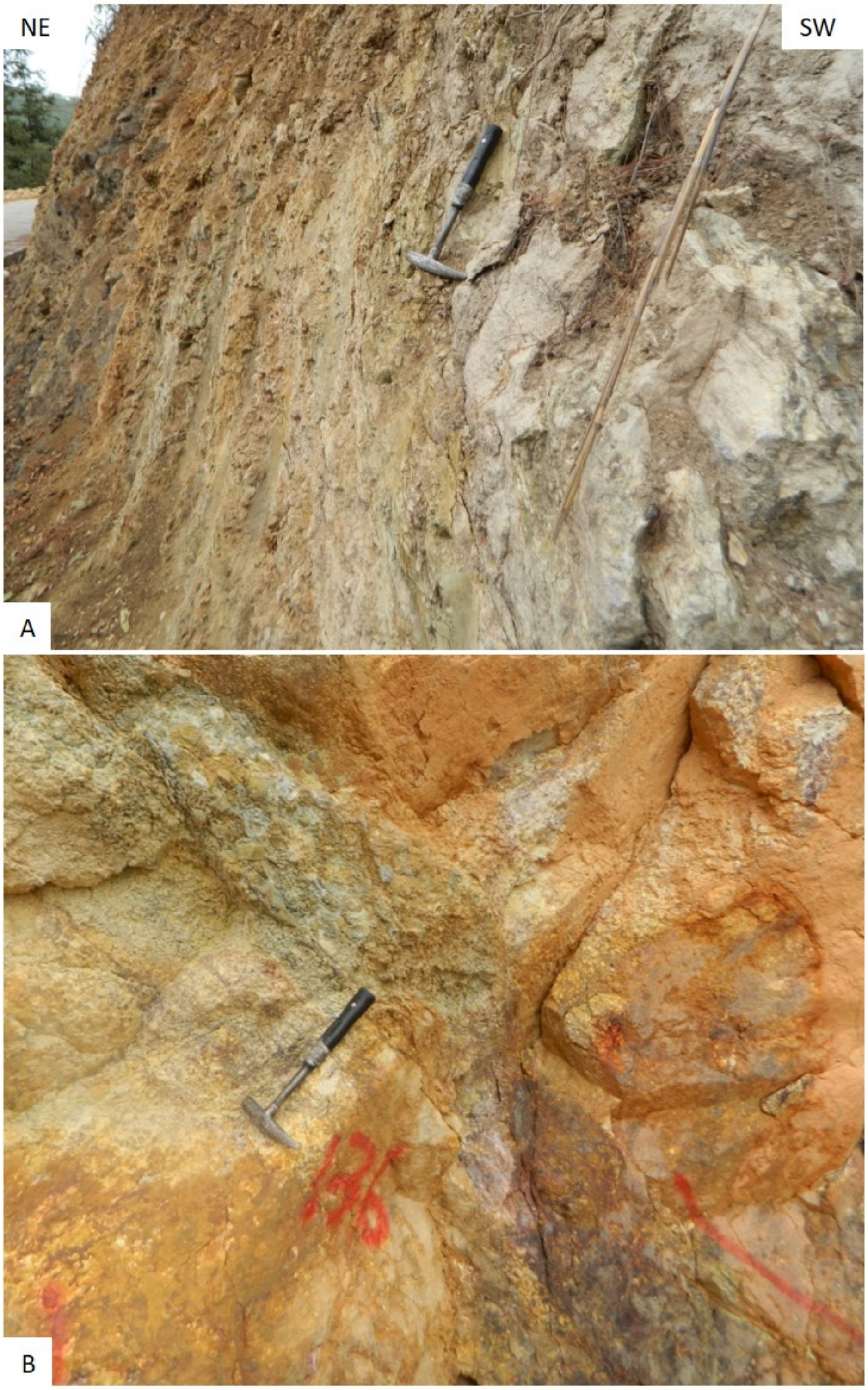

Figure 13

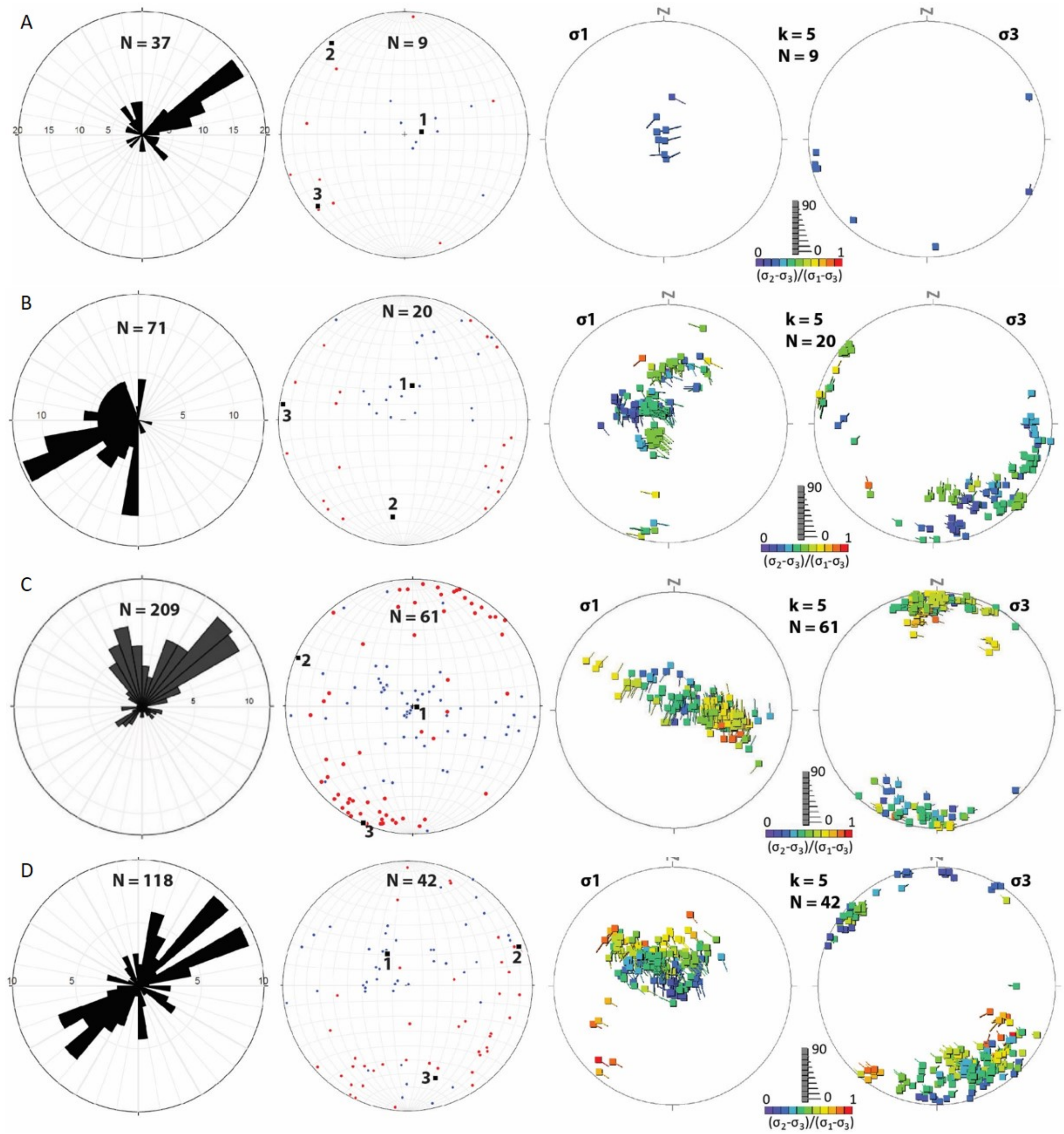

A
N = 37
N = 9
σ1
k = 5
N = 9
σ3
B
N = 71
N = 20
σ1
k = 5
N = 20
σ3
C
N = 209
N = 61
σ1
k = 5
N = 61
σ3
D
N = 118
N = 42
σ1
k = 5
N = 42
σ3
(σ2-σ3)/(σ1-σ3)

Figure 14

Figure 15

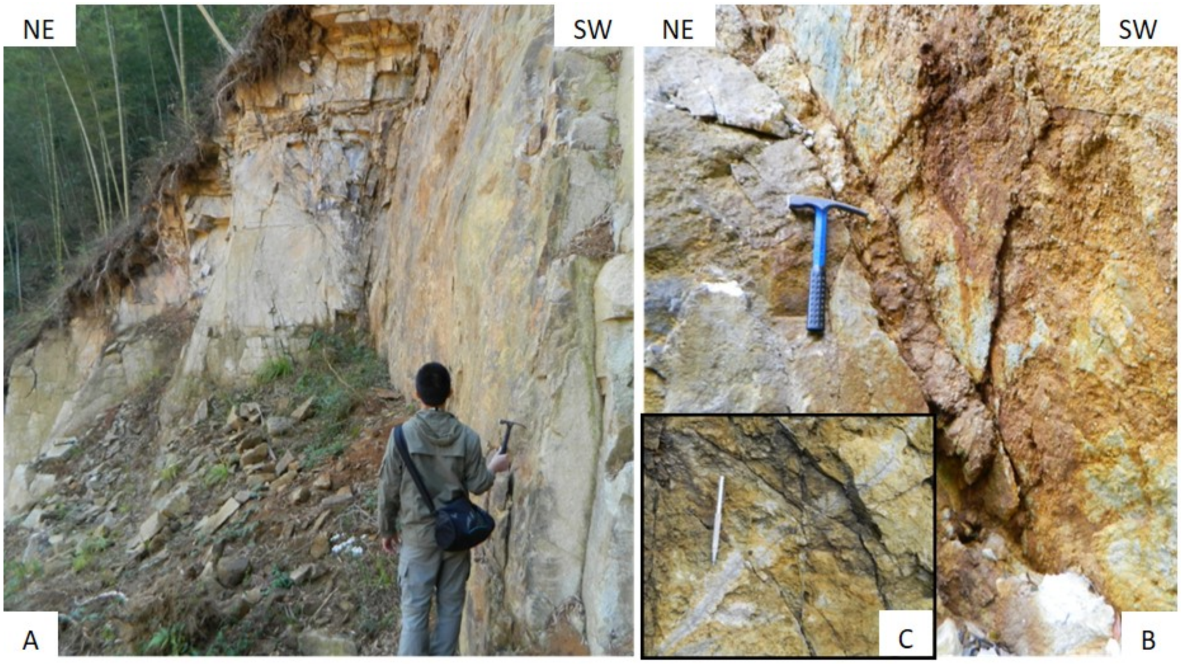

Figure 16

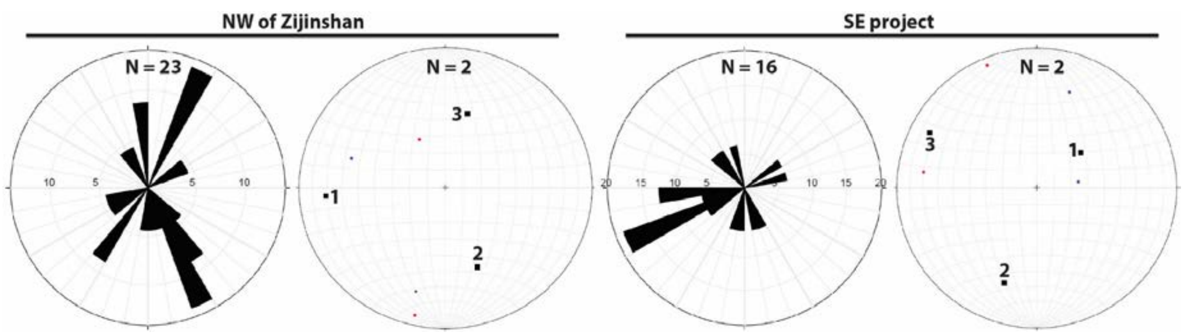

Figure 17

Table 1. Summary of magmatic and hydrothermal events recognized in the study area

Intrusive events	**Volcanic events**	**Hydrothermal events**
Jingmei, Wulongzi and Jinlongqiao granites 165 - 157 Ma *U-Pb in zircons; Jiang et al. (2013)*		
Sifang granodiorite 113 - 111 Ma *U-Pb in zircons; Jiang et al. (2013)*		
Dacitic domes and dikes 110 - 104 Ma *U-Pb in zircons; Jiang et al. (2013)*	Volcanic rocks of the Shimaoshan Group 110 - 99 Ma *U-Pb in zircons Jiang et al. (2013, 2015)*	
Luoboling granodiorite porphyry 106 - 103 Ma *Whole rock Rb-Sr, U-Pb in zircons; Zhang et al. (2001); Li and Jiang (2015)*		Porphyry-style mineralization 106 - 103 Ma *Re-Os in molybdenite; Zhong et al. (2014)*
Syenite and quartz-monzonite dikes 100 - 92 Ma *U-Pb in zircons; Li and Jiang (2014)*		Intermediate-sulfidation epithermal mineralization 97 - 91 Ma *$^{40}Ar/^{39}Ar$ in adularia; Zhang et al. (2003); Liu and Hua (2005)*